TÉCNICO LISBOA

A contribution to further understand the molecular mechanisms of antifungal resistance in *Candida glabrata* mediated by the transcription factor CgPdr1

Rita Silva Ramos Madureira Simões

Thesis to obtain the Master of Science Degree in

Biotechnology

Supervisor: Prof. Dr. Nuno Gonçalo Pereira Mira

Examination Committee

Chairperson: Prof. Dra. Leonilde de Fátima Morais Moreira

Supervisor: Prof. Dr. Nuno Gonçalo Pereira Mira

Member of the Committee: Prof. Dra. Sónia Carina Morais Silva

October 2018

Acknowledgements

First of all, I would like to thank my supervisor Professor Nuno Mira for taking me in at the Institute for Bioengineering and Biosciences (iBB), Instituto Superior Técnico (IST), University of Lisbon, where the great majority of my work was conducted. Since day one, Professor Nuno Mira never failed to guide and encourage me, and throughout my scientific experiments and the elaboration of this thesis he always presented helpful solutions and an unwavering enthusiasm to overcome the obstacles that arose, even when the obstacle were my own paranoias.

Moreover, I would like to express my gratitude to Professor Isabel Sá-Correia for providing the necessary conditions to realize this thesis within the Biological Sciences Research Group (BSRG) and for her help and support in other activities that accompanied my thesis. My acknowledgements are also going to Professor Fernanda Carvalho from the Centro de Química Estrutural (IST), for kindly and ever so patiently synthesizing the chemical compounds used in this thesis. Moreover, I would like to thank Professor Dr. Manuel Santos for allowing me to conduct part of my studies at the iBiMED, Universidade de Aveiro, and Dra. Ana Raquel Soares for assisting me in the analysis of my results. I also would like to acknowledge the funding received by iBB-Institute for Bioengineering and Biosciences from FCT-Portuguese Foundation for Science and Technology (UID/BIO/04565/2013), from Programa Operacional Regional de Lisboa 2020 (Project N. 007317).

When I first arrived at my lab I could never have imagined how important my colleagues would be in the completion of my work and in the maintenance of my mental sanity. Hence, I would like to thank Sara Salazar for her patience in guiding me in the lab when I first arrived (and in all the months that followed), Pedro Pais and Mafalda Cavalheiro whom I always bothered with questions whenever Sara wasn't around, Tiago Brito for passing down all his molecular biology skills and for his companionship and humorous attitude which helped shine a light over darker times, and José António Souza for being my partner on the road to Aveiro and for always keeping me cheerful. I am very grateful for all my colleagues at the BSRG group who welcomed me to their little family and made sure that I never felt alone.

Furthermore, I want to thank all my friends outside the lab who accompanied me since the first day of this master's, sharing and attenuating my growing pains: Alexandra Balola, Cristiana Ulpiano, João Carvalho, João Lampreia, Jorge João, Mariana São Pedro, Pedro Monteiro, Raquel Califórnia, Rodrigo Pedroso and Susana Vagueiro. A special shout out goes to Inês Sá and Diogo Reis who possess an amazing gift that allows them to spit in the face of adversity and always be positive that everything will work out, needless to say that without them this project would never have been complete.

Additionally, I would like to appreciate my family who, in spite of being clueless of my work for most of the times, never failed to remind me of how far I've come and how proud they were of my accomplishments. Specially my mom and dad who taught me to be strong and never give up, my grandparents who always valued my work and effort, and my sister who, in spite of all the nagging and disagreements, is secretly one of my biggest fans. I am thankful because I know it was hard but they never gave up on me and always made sure I had everything I needed.

Finally, I want to say a special thank you to Gonçalo, my best friend and lifetime companion. For his tireless support in times of trouble, for all the effort he took (as a law major) to understand my scientific work, for all the laughter when sadness insisted in persisting, for all the car rides late in the night and after a hard day of work so I could stay a few more hours and complete my research, for all the snacks that fueled my sugar rampages due to stress and for all the love that he gave me which kept me sane and inspired.

Abstract

Recently, *Candida glabrata* has emerged as a human pathogen, partly due to its high resilience to azoles which has been shown to result, generally, from the acquisition of point mutations in the transcriptional regulator CgPdr1 that render the protein constitutively active, even in the absence of any drug. In this work three non-characterized mutations in *CgPDR1* – E5K, R35K and I392M – were identified in azole-resistant clinical isolates. Expression profiling of *CgCDR1* and *CgPUP1*, two hallmarks of CgPdr1 hyper-activity, and site-directed mutagenesis strongly suggested that E5K and I392M are new gain-of-function CgPdr1 substitutions resulting in azole resistance. Additionally, it was investigated how gain-of-function substitutions modulate the biochemical activity of CgPdr1 and, specially, its transactivation potential.

The increasing emergence of azole-resistant *C. glabrata* strains and the recently shown anti-*C.glabrata* efficacy of Ag(I)-camphorimine complexes outlined this work's remaining objectives: i) characterize how these complexes affect the physiology of *C. glabrata*; ii) search for new Ag(I)-derived compounds showing anti-*C.glabrata* potential, including against azole-resistant strains. DNA microarrays revealed that exposure to compound A results in up-regulation of genes involved in oxidative stress response and methionine metabolism, simultaneously leading to down-regulation of genes involved in glucose and iron uptake. Although further studies are required, the results obtained show that the effects of Ag(I)-camphorimine complexes are similar to those already described for silver. Two novel compounds, B and C, were also herein characterized as robust anti-*C.glabrata* agents, against both laboratory (MIC=62,5 mg/L) and azole-resistant (MIC between 125-500 mg/L) strains, reinforcing the usefulness of these chemicals as new antifungals.

Key-words: *Candida glabrata* • CgPdr1 • Resistance • Antifungals • Gain-of-function mutations • Ag(I)-camphorimine complexes

Resumo

Recentemente, *Candida glabrata* emergiu como patógeno humano em parte devido à sua elevada resiliência aos azóis, resultante, em muitos casos, da aquisição de mutações pontuais no regulador transcricional CgPdr1 que tornam a proteína constitutivamente ativa, mesmo na ausência de drogas. Neste trabalho foram identificadas três mutações não-caracterizadas - E5K, R35K e I392M - no *CgPDR1* de isolados clínicos resistentes a azóis. Os perfis de expressão de *CgCDR1* e *CgPUP1*, dois genes associados à hiperatividade de CgPdr1, e a mutagénese dirigida evidenciaram E5K e I392M enquanto novas substituições de ganho-de-função em CgPdr1 conducentes à resistência aos azóis. Adicionalmente, foi investigado o modo como as substituições de ganho-de-função modulam a atividade bioquímica do CgPdr1 e o seu potencial de transactivação.

O crescente número de isolados clínicos de *C. glabrata* resistentes aos azóis e a eficácia anti-*C.glabrata* recentemente demonstrada de complexos de Ag(I)-camforimina motivaram os dois outros objetivos deste trabalho: i) caracterizar o efeito destes complexos na fisiologia de *C. glabrata*; ii) investigar novos compostos à base de Ag(I)-camforimina com potencial anti-*C.glabrata*, inclusive contra isolados resistentes aos azóis. Microarrays de DNA revelaram que a exposição ao composto A resulta na sobre-expressão de genes envolvidos na resposta ao stress oxidativo e no metabolismo da metionina, simultaneamente conduzindo à sub-expressão de genes envolvidos no transporte de glucose e ferro. Embora seja necessária uma análise mais aprofundada, os resultados obtidos revelam semelhanças entre os efeitos dos complexos de Ag(I)-camforimina e aqueles já descritos para a prata. Dois novos compostos, B e C, foram também caracterizados neste trabalho como tendo um forte efeito inibitório contra estirpes de *C. glabrata* laboratoriais (MIC=62,5 mg/L) e resistentes a azóis (MIC entre 125-500 mg/L), reforçando a relevância destes compostos como novos antifúngicos.

Palavras-chave: *Candida glabrata* • *CgPDR1* • Resistência a antifúngicos • Mutações ganho-de-função • Complexos de Ag(I)-camforimina

Table of contents

Acknowledgements II
Abstract IV
Resumo V
Table of contents VI
List of figures VIII
List of tables XI
Abbreviations XIII
1. Introduction 1
1.1. Overview 1
1.2. Emergence of *Candida glabrata* as a medically relevant infectious agent 2
1.3. Antifungal drugs - current treatment solutions 2
1.3.1. Azoles: ergosterol synthesis inhibitors 3
1.4. Molecular mechanisms underlying *C. glabrata* resistance to azoles 4
1.4.1. The CgPdr1 network and its involvement in azole resistance in *C. glabrata* 5
1.5. The acquisition of gain-of-function CgPdr1 mutations as a driver of *C. glabrata* resistance to azoles 7
1.6. Novel antifungal therapies 9
1.7. Introduction to the theme of the thesis 12
2. Materials and Methods 13
2.1. Strains and growth media 13
2.2. Preparation of Ag(I)-derived chemicals 13
2.3. Yeast genomic DNA extraction 14
2.4. Cloning of various CgPdr1 constructs to assess their biochemical activity 14
2.5. Microdilution assays 15
2.6. Growth curves in the presence of the Ag(I)-derived chemicals 16
2.7. RNA extraction and microarrays 16
2.8. Assessment of gene expression based on real time RT-PCR 17
2.9. RNA extraction (phenol method) 19
2.10. Site-directed Mutagenesis 19
2.11. Classical Transformation of *E. coli* DH5α competent cells 20
2.12. Sanger sequencing of *CgPDR1* gene of azole-resistant isolates 21
2.13. Growth curves in the presence of Fluconazole 21
3. Results and Discussion 22
3.1. Unveiling novel gain-of-function mutations in *CgPDR1* 22
3.2. Assessing the role of candidate CgPdr1 GOF mutations in the azole-resistance phenotype of *C. glabrata* and *S. cerevisiae* 24
3.3. Unraveling the role of GOF mutations in the biochemical activity of CgPdr1 27
3.4. Transcriptomic analysis of *C. glabrata* cells grown in the presence of the Ag(I)-derived compound A 29

3.5. Efficacy of new Ag(I)-derived compounds against *C. glabrata* 35
4. Concluding remarks 40
5. References 42
6. Annexes 47
Annex A 47
Annex B 48
Annex C 49
Annex D 50
Annex E 51
Annex F 52
Annex G 53

List of figures

Figure 1.1 - Antifungal drug classes and their respective targets and modes of action in the fungal cell. 3

Figure 1.2 - Comparison of documented fluconazole resistance mechanisms in various *Candida* species (in Whaley *et al.*, 2017). [29] 4

Figure 1.3 - Functional domains of zinc cluster proteins and of the CgPdr1 transcription factor. 6

Figure 1.4 - Schematics depicting the activation of CgPdr1 in response to the exposure to drugs (adapted from Goffeau, 2008 [45]). 7

Figure 1.5 - Schematics compiling the *C. glabrata* PDR1 gain-of-function mutations described in Tsai *et al.*, 2006 [33], Torelli *et al.*, 2008 [48], Ferrari *et al.*, 2009 [39], Berila *et al.*, 2009 [49], Tsai *et al.*, 2010 [27], Caudle *et al.*, 2011 [31] and Salazar *et al.*, 2017 [50]. The illustration of the CgPdr1 domains was done using the Illustrator for Biological Sequences online tool (available at http://ibs.biocuckoo.org/online.php). 8

Figure 1.6 - Venn diagram comparing the set of genes regulated by the CgPdr1 GOF mutants K274Q, K274N, P927L and L946S, as revealed by transcriptomic analyses (retrieved from Salazar *et al.*, 2017 [50]). From the analysis of overlaps between GOF mutants it is possible to conclude that different amino acid substitutions clearly generate distinct transcriptomic responses. 9

Figure 1.7 – MIC values (μg/mL) for Ag(I) camphor complexes 1–8 and for $AgNO_3$ against *C. albicans*, *C. glabrata*, *C. tropicalis* and *C. parapsilosis*, based on the EUCAST microdilution method (retrieved from Cardoso *et al.*, 2017 [56]). 10

Figure 1.8 - Camphorimine complexes used as ligands of the compounds tested in this thesis. Ligand 1 is made up of camphor and lithium and it was used in the synthesis of compounds B and C. Ligand 3 is a camphor di-imine and was used to synthesize compound A. 12

Figure 2.1 – Microdilution methodology used in this work. 16

Figure 3.1 - Comparison of the transcript levels of *CgCDR1* and *CgPUP1* genes in various azole-resistant isolates. Cells of the different isolates were cultivated in RPMI growth medium until mid-exponential phase, after which the expression of *CgCDR1* and *CgPUP1* genes was compared by qRT-PCR. The values represented for each isolate are relative to the value obtained for the CBS138 strain, which was considered to be equal to 1. Gene expression was calculated using *RDN25* as an internal control. 23

Figure 3.2 – Map depicting the features of plasmid pSP76. 24

Figure 3.3 - Growth curves of the various *S. cerevisiae* wild-type and Δ*pdr1* mutant transformants when in presence of fluconazole concentrations ranging between 8,00 – 64,00 mg/L. 25

Figure 3.4 - Growth curves of the various *C. glabrata* wild-type and Δ*pdr1* mutant transformants when in presence of fluconazole concentrations ranging between 8,00 – 64,00 mg/L. 26

Figure 3.5 - A) Schematics depicting the features of vector pYEF2-DBD_Haa1_VP16; B) Structural domains of the CgPdr1 transcription factor and the various protein constructs elaborated to assess its biochemical activity; C) PCR amplification to obtain the fragments corresponding to three CgPdr1 constructs: DBD, DBD+GOFs and DBD+GOFs+RD; D) PCR amplification to obtain the fragments corresponding to the two segments of the DBD+RD construct; E) Gel

electrophoresis depicting the pYEF2-DBD_Haa1_VP16 digested with BamHI and ClaI; F) Restriction digest of the DNA extracted from candidates containing the DBD construct with BamHI and ClaI. 28

Figure 3.6 - A) Growth curves of *C. glabrata* CBS138 strain in the presence (•) and absence (■) of compound A. The red arrows mark the time-point (t=1 hour) selected to perform cell harvest for later RNA extraction. B) Colony forming units per milliliter calculated for each tested condition over a 24-hour period. 29

Figure 3.7 - Graphical representation of the relative frequency of the main biological functions found to be enriched in the set of genes up-regulated (up) or down-regulated (down) in *C. glabrata* cells upon exposure to compound A. 31

Figure 3.8 - A) Microdilution assays performed using *C. glabrata* and *C. parapsilosis* at pH 5 and 7 to determine if ethanol alone had an inhibitory effect; B) Microdilution assays performed using *C. glabrata* and *C. parapsilosis* at pH 5 and 7 to determine if the ligand 1 alone had an inhibitory effect; C) Microdilution assays performed using *C. glabrata* and *C. parapsilosis* at pH 5 and 7 to determine the inhibitory effect of compound B; D) Microdilution assays performed using *C. glabrata* and *C. parapsilosis* at pH 5 and 7 to determine the inhibitory effect of compound C. The red lines mark the cell density correspondent to 50% of the full population. 36

Figure 3.9 - Microdilution assays performed using three azole-resistant *C. glabrata* isolates – FFUL412, FFUL443 and FFUL674 – at pH 5 and 7 to determine the inhibitory effect of compounds B and C. Cells were also grown in the presence of ethanol to determine if this chemical alone had any inhibitory potential. The red lines mark the cell density correspondent to 50% of the full population. 37

Figure 3.10 - Microdilution assays performed using three azole-resistant *C. glabrata* isolates – FFUL830, FFUL866 and FFUL887– at pH 5 and 7 to determine the inhibitory effect of compounds B and C. Cells were also grown in the presence of ethanol to determine if this chemical alone had any inhibitory potential. The red lines mark the cell density correspondent to 50% of the full population. 38

Figure 6.1 - Alignment of the *CgPDR1* sequence obtained from isolate FFUL29 with the sequence of the CBS138 reference strain. The sequencing reaction was performed by STABVIDA as a paid service and Clustal Omega was used for sequence alignment. Amino acid substitutions are represented by a red rectangle. 48

Figure 6.2 - Alignment of the *CgPDR1* sequence obtained from isolate FFUL56 with the sequence of the CBS138 reference strain. The sequencing reaction was performed by STABVIDA as a paid service and Clustal Omega was used for sequence alignment. Amino acid substitutions are represented by a red rectangle. 49

Figure 6.3 - Alignment of the *CgPDR1* sequence obtained from isolate FFUL556 with the sequence of the CBS138 reference strain. The sequencing reaction was performed by STABVIDA as a paid service and Clustal Omega was used for sequence alignment. Amino acid substitutions are represented by a red rectangle. 50

Figure 6.4 - Alignment of the *CgPDR1* sequence obtained from isolate FFUL607 with the sequence of the CBS138 reference strain. The sequencing reaction was performed by STABVIDA as a paid service and Clustal Omega was used for sequence alignment. Amino acid substitutions are represented by a red rectangle. 51

Figure 6.5 - Growth curves of the various *S. cerevisiae* and *C. glabrata* transformants, wild-type and ∆pdr1 mutant variants, when in the absence of fluconazole. 53

List of tables

Table 1.1 - Alternatives to current antifungals used in clinical practice developed over the last years along with their descriptions and mode of action. 11

Table 2.1 - Description of the group of strains used in this work. 13

Table 2.2 - Primers used for the amplification of the DNA correspondent to each CgPdr1 construction. The underlined nucleotides correspond to the sequence that will allow digestion with the restriction enzyme indicated in the primer ID. The nucleotides marked in bold will allow the obtainment of the DBD+RD construct by overlapping PCR. 14

Table 2.3 - PCR reaction mixture used amplify the CgPdr1 constructs. 15

Table 2.4 - Conditions of the PCR cycles for amplification of the CgPdr1 constructs. The extension time was calculated using a calculus basis of 30 s per kilobase of the amplified fragment. 15

Table 2.5 – Reaction mixture used to insert each construct into the pYEF2-DBD_Haa1_VP16 plasmid. 15

Table 2.6 - PCR reaction mixture used for each strain in order to obtain cDNA. 18

Table 2.7 - Conditions of the PCR cycles for obtainment of cDNA. 18

Table 2.8 - RT-PCR reaction mixture. 18

Table 2.9 - Sequences of the primers used to perform RT-PCR. 18

Table 2.10 - Sequences of the primers used for site-directed mutagenesis. 19

Table 2.11 - PCR reaction mixture used in order to obtain the desired mutations. 20

Table 2.12 - Conditions of the PCR cycles for site-directed mutagenesis. 20

Table 2.13 - Primer sequences used to amplify the selected regions of *CgPDR1* gene containing the desired mutations. 20

Table 2.14 - Sequences of the primers used to sequence the *CgPDR1* of isolates FFUL29, FFUL56, FFUL556 and FFUL607. 21

Table 3.1 - Alterations in the amino acid sequence of CgPdr1 transcription factor encoded by the azole-resistant isolates when compared to the CgPdr1 encoded by the CBS138 strain. The non-synonymous SNPs associated with a resistance phenotype were marked in red, the susceptible non-synonymous SNPs were marked in green and the non-described non-synonymous SNPs were marked in blue. The candidates to be new GOF variants of CgPdr1 were marked with an asterisk (*).The described mutations were retrieved from Ferrari *et al.*, 2009 [39], Caudle *et al.*, 2011 [31], Katiyar *et al.*, 2016 [68], and Salazar *et al.*, 2017 [50]. 22

Table 3.2 - Main functional categories identified by the MIPS Functional Catalogue Database tool (p-value <0,05) as up-regulated in the presence of compound A, alongside with the major genes within each category, their fold-change when compared to the control condition, and their description as provided by PathoYEASTRACT. 32

Table 3.3 - Main functional categories identified by the MIPS Functional Catalogue Database tool (p-value<0,05) as down-regulated in the presence of compound A, alongside with the major genes within each category, their fold-change when compared to the control condition, and their description as provided by PathoYEASTRACT. 33

Table 6.1 - List of clinical isolates used in this thesis, the samples from which they were collected, and fluconazole and/or voriconazole minimal inhibitory concentration (in mg/L). ND – No data available..... 47

Table 6.2 - List of transformed strains obtained upon insertion of the wild-type or mutated pSP76 vector into *S. cerevisiae* BY4741, *S. cerevisiae* BY4741 Δ*pdr1*, *C. glabrata* Cg66032 or *C. glabrata* SKY107..... 52

Abbreviations

ABC	ATP-Binding Cassette
AD	Activation Domain
C. albicans	*Candida albicans*
C. glabrata	*Candida glabrata*
C. parapsilosis	*Candida parapsilosis*
cDNA	Complementary Deoxyribonucleic acid
CFU	Colony Forming Units
DBD	DNA Binding Domain
ddH_2O	Double Distilled Water
DMSO	Dimethyl Sulfoxide
DNA	Deoxyribonucleic Acid
dNTP	Deoxyribonucleotide Triphosphates
E. coli	*Escherichia coli*
EtOH	Ethanol
EUCAST	European Committee on Antimicrobial Susceptibility Testing
FLC	Fluconazole
FW	Forward
GOF	Gain-of-function
MMB	Modified Medium B
MDR	Multi-drug Resistance
MFS	Major Facilitator Superfamily
MHR	Middle Homology Region
MIC	Minimum Inhibitory Concentration
NCAC species	Non-*Candida albicans Candida* species
OD	Optical Density
ORF	Open Reading Frame
PDR	Pleiotropic Drug Resistance
PDRE	Pleiotropic Drug Response Element
RD	Regulatory Domain
RNA	Ribonucleic Acid
RPM	Rotations per minute
RPMI	Roswell Park Memorial Institute
RT-PCR	Reverse Transcription Polymerase Chain Reaction
RV	Reverse
S. cerevisiae	*Saccharomyces cerevisiae*
spp.	Species
YPD	Yeast Peptone Dextrose

1. Introduction

1.1. Overview

Yeasts belonging to the genus *Candida* are eukaryotic, unicellular microorganisms, widely distributed in nature, being normally found as commensal organisms on mucosal and cutaneous surfaces throughout the human body. [1] This commensalism carries numerous advantages for the *Candida* species, which are able to proliferate without causing significant damage to their host. Thereby, *Candida* spp. rarely trigger infection in healthy individuals, instead taking advantage of an impaired immune system to proliferate within the host, resulting in an extensive colonization of mucosal surfaces or of the bloodstream, depending on the seriousness of the infection. [2, 3] The clinical manifestations of candidiasis can be classified as acute or chronic, and as superficial or invasive. Superficial infections affect the skin or mucous membranes whilst invasive candidiasis is usually systemic, arising when yeast cells reach the bloodstream, where they may end up colonizing either of the main internal organs. [2, 4, 5]

The incidence of fungal infections has risen over the past decades, now emerging as one of the main public health concerns and with *Candida* spp. being ranked as the fourth main cause of bloodstream infections in hospitals. [6] Moreover, invasive infections caused by species of the *Candida* genus are responsible for more fatalities than any other systemic mycosis, having an associated mortality of approximately 40%. [7] Although epidemiological reports show that *C. albicans* remains the most frequently isolated agent of candidiasis, non-*Candida albicans Candida* (NCAC) species now account for a substantial part of the candidiasis infections reported worldwide in hospitals, with *Candida glabrata* currently being the second most prevalent yeast pathogen in humans. [2] A highly relevant trait presumed to be an important factor underlying the success and emergence of *C. glabrata* as a pathogen is its intrinsic high resilience to fluconazole, the frontline drug used for both active and prophylactic treatments of candidiasis. [8] Furthermore, this species has also been shown to acquire resistance to antifungals at a higher rate than any other *Candida* spp. [8]

Alternative antifungals structurally different from azoles and with distinct biological targets (e.g. echinocandins or polyenes) are available in clinical practice, however these are in general much more expensive and in some cases present higher toxic effects [9] for the patients thereby rendering their utilization as prophylactic agents very difficult. Moreover, the number of strains resistant to these drugs is rising [10] aggravating the prognosis of patients infected with these isolates given that it becomes increasingly difficult to eliminate the pathogen. Taken together, these data highlight the importance of properly understanding the mechanisms underlying the development of acquired resistance to azoles.

Various studies [8, 11, 12] focused on different cohorts of azole-resistant *C. glabrata* strains have shown an essential role of the transcriptional regulator CgPdr1 in mediating the observed resistant phenotype. Unveiling the molecular mechanisms underlying the CgPdr1-mediated azole resistance of *C. glabrata* would allow the improvement of currently used antifungals by targeting this transcription factor. The deepening of this knowledge would also facilitate the identification of azole-resistant clinical isolates eliminating the costs that often accompany a delayed diagnosis. Alternatively, the development of novel antifungal drugs with modes of action mechanistically distinct from those of

current antifungals, would boost current clinical therapies, especially if these drugs prove to be efficient when used alone or combined with other antifungals.

1.2. Emergence of *Candida glabrata* as a medically relevant infectious agent

Over the past 20 years the epidemiology of infections caused by *Candida* spp. has been changing, following the tendency already observed in other types of fungal infections for which the incidence has progressively increased and species once considered harmless, non-pathogenic or less virulent are now recognized as a primary cause of morbidity and mortality in immunocompromised and severely ill patients. [13, 14]

Although *Candida albicans* remains the most prevalent species involved in both muco-cutaneous and disseminated infections, the incidence of infections attributed to *non-Candida albicans Candida* (NCAC) species is clearly increasing. [13] Whereas NCAC species accounted for 10% to 40% of all systemic candidiasis from 1970 to 1990, this proportion reached 35% to 65% only in the last two decades. [2] A recent ten-year analysis of the worldwide distribution of NCAC species indicated that *C. glabrata* remains the most frequently isolated species, reinforcing its emergence as a human pathogen. [15] Various factors are reported to be associated with this change, namely the excessive use of azoles, (particularly fluconazole) which was actively applied both as prophylaxis and in the treatment of fungal infections in patients, resulting in the selection of more tolerant NCAC species. [14] Another contributing factor was the development of more sensitive species identification methods, which allowed a more accurate distinction of clinical isolates. [16]

Despite the scarcity of epidemiological data regarding fungaemias in Portugal, there are some studies that allow us to shed some light over the matter. Overall, a total of 231 cases of candidaemia are estimated per year [17] with reports [18] of numerous different *Candida* species being identified, among which *C. albicans* (40%) was the most prevalent, followed by *C. parapsilosis* (23%) and *C. glabrata* (13%). Other studies [19, 20] report *Candida glabrata* as the second most frequently isolated species and the one with the highest mortality value associated. Regarding susceptibility to antifungals, *C. glabrata* has been documented [18] as exhibiting the highest percentage of resistance to fluconazole when compared to other *Candida* species, reaching minimal inhibitory concentration (MIC) values of 64 mg/L for this drug whilst *C. albicans* and *C. parapsilosis* both presented a MIC value of 8 mg/L. In conclusion, these data unveil the fact that NCAC species are emerging as the leading cause of candidiasis in Portugal, with *C. glabrata* among the most commonly isolated species.

1.3. Antifungal drugs - current treatment solutions

Antifungal drugs act by exploiting the differences between mammalian and fungal cells, in order to eradicate the fungal organism with the least adverse effects possible to the host. Unfortunately, fungal and human cells are both eukaryotic and quite are similar at a biological level, which significantly hinders the discovery of drugs that target fungi without affecting human cells. As a consequence, many antifungal drugs cause side-effects in humans, some of which can even worsen the patient's initial state of sickness. There are currently several classes of antifungal drugs available in the market, each varying in their chemical composition and biological target. A brief representation

of these drugs and of their biological targets is provided in Figure 1.1., however since this thesis was focused on azoles, the following sections will be dedicated to those drugs.

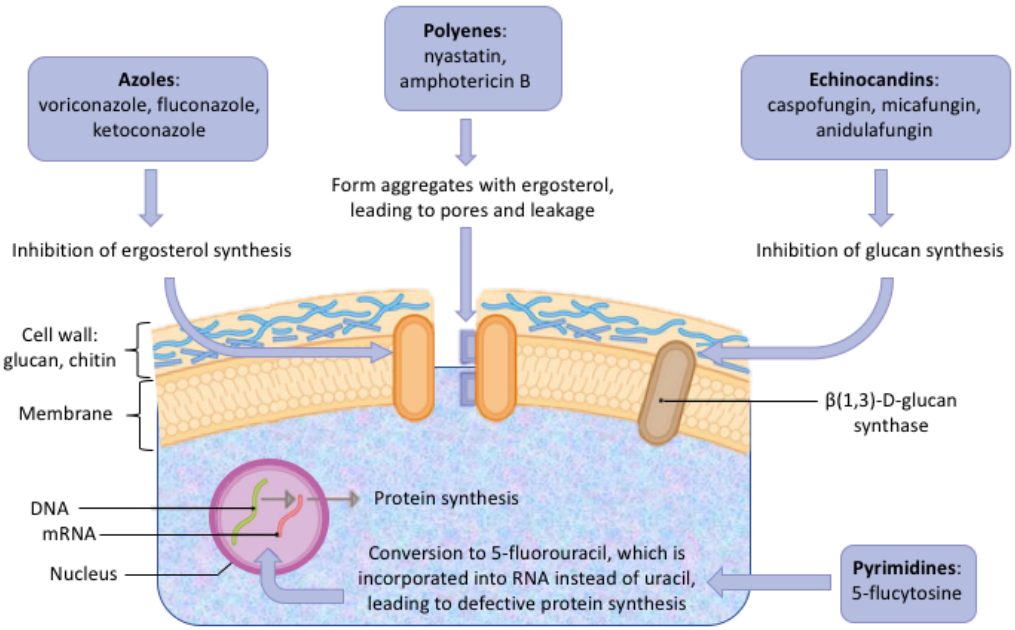

Figure 1.1 - Antifungal drug classes and their respective targets and modes of action in the fungal cell.

1.3.1. Azoles: ergosterol synthesis inhibitors

Since the late 1960's that antifungal azoles have been in use in clinical practice, nowadays being the class of antimycotics comprising the highest number of compounds. Azoles can be classified as first, second or third generation, depending on their structure. Compounds of the first generation, such as ketoconazole, contain imidazole in their ring system and are mainly applied topically due to their poor water solubility and adverse side-effects if administered orally. The second (e.g. fluconazole) and third (e.g. voriconazole) generation azoles possess a triazole ring and present lower toxicity due to their increased affinities to the target enzyme in the invading pathogen as compared with the antifungal imidazoles. [21]

The mechanism of action of all antifungal azoles is based on the inhibition of the fungal cytochrome P450 from family 51 (CYP51 or sterol 14α-demethylase) that is essential for the biosynthesis of ergosterol. Ergosterol is the major component of the fungal cellular membrane, acting as a bioregulator of membrane fluidity, asymmetry and integrity. The blockage of sterol 14α-demethylase activity has three major effects: ergosterol depletion, changes in membrane permeability and in the activity of membrane-bound proteins, and accumulation of toxic sterols. Since ergosterol plays a hormone-like role in fungal cells, stimulating growth, the net effect of azoles is the inhibition of the fungal growth. [22, 23]

The sterol 14α-demethylase is encoded by the *ERG11* gene in *Candida glabrata* and it removes the 14α-methyl group from lanosterol, which is one of the last steps in the biosynthesis pathway of ergosterol. [11] While in most *Candida* species the inhibition of *ERG11* by exposure to azoles leads to

the accumulation of the toxic sterol 14α-methyl-3,6-diol [24], in *C. glabrata* the sterols accumulated are slightly different and they are non-toxic. Additionally, whilst several *Candida* spp. acquire mutations in the *ERG11* gene as a target modification mechanism to resist azoles, *C. glabrata* does not commonly exhibit these mutations and, even when it does, they appear not to be directly correlated with an increased resistance of isolates to azoles. [25, 26] Additionally, mutations on the *ERG11* gene or even its deletion in *C. glabrata* do not render the strain more susceptible to azoles than the wild-type nor do they make it significantly more resistant to these compounds. [27] Therefore, *Candida glabrata* exhibits an inherent resistance to azoles, a trait not shared with other *Candida* species and one that certainly conveys a challenge for clinical therapies.

1.4. Molecular mechanisms underlying *C. glabrata* resistance to azoles

Antifungal drugs act on specific cellular targets, compromising the growth or the survival of fungi. However, fungi have developed several mechanisms that provide them the ability to overcome the inhibitory action of antifungal drugs and, hence, survive and thrive even in the presence of these compounds. [28] As previously mentioned in this thesis, one of the mechanisms employed by *C. glabrata* to overcome azole exposure lies on the ability of this pathogen to bypass the accumulation of toxic sterols.

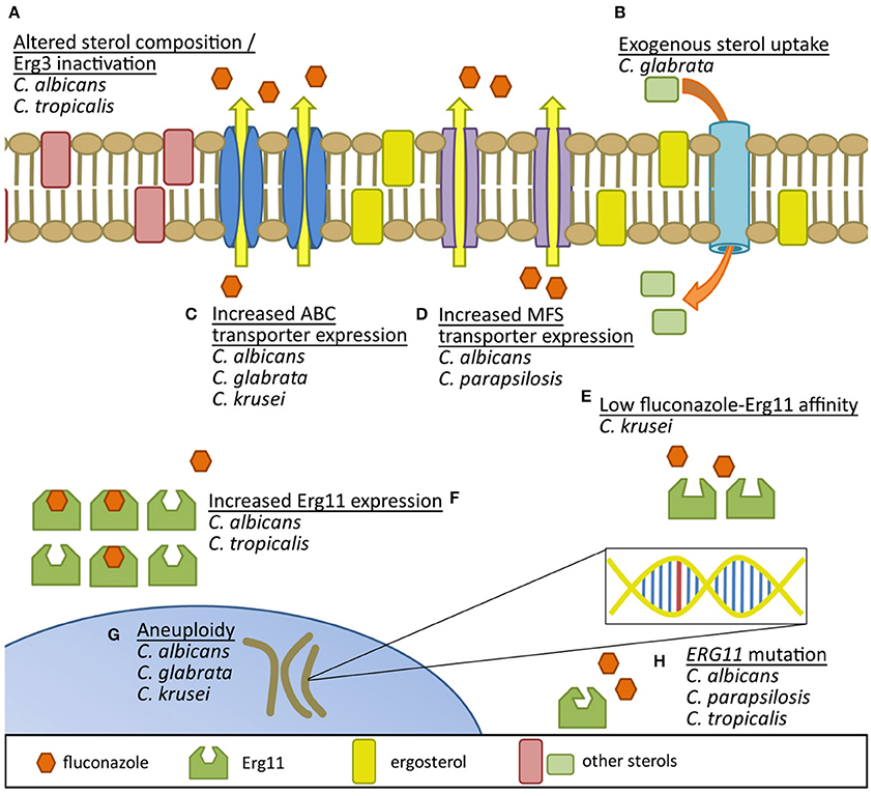

Figure 1.2 - Comparison of documented fluconazole resistance mechanisms in various *Candida* species (in Whaley *et al.*, 2017). [29]

Another mechanism put in place by *C. glabrata* cells when exposed to azoles consists on the discharge these compounds to the extracellular medium. The active efflux from yeast cells strongly modulates the activity of a large number of antifungals and, even though there are numerous efflux

pumps in a fungal cell, only a few have been linked to drug resistance. Those involved in the transport and extrusion of azoles belong to two main classes: ATP-binding cassette (ABC) and major facilitator superfamily (MFS). [11] In *C. glabrata*, the multi-drug efflux pumps of the ABC Superfamily implicated in tolerance to azoles are *CgCDR1*, *CgPDH1*, *CgPDR16* and *CgSNQ2*. Consistent with this, *C. glabrata* clinical isolates resistant to azoles were found to exhibit significantly higher expression levels of the genes expressing CgCDR1, CgPDH1 and CgSNQ2, when compared to the expression levels registered in susceptible isolates. [11, 12] The role of the MFS multidrug resistance transporters in *C. glabrata* tolerance to azoles has been much less studied, comparing with ABC transporters, and only recently has the important role of this protein family for the azole-resistance phenotype been examined. Three MFS transporters were identified and characterized in what concerns their contribution to *C. glabrata* azole resistance: CgQdr2, CgAqr1, and CgTpo3. [30] The expression of *CgQDR2* had been previously shown to be increased in a clinical isolate exhibiting fluconazole resistance [31], however, more recently, the genes encoding these three MFS transporters were shown to be significantly up-regulated in clotrimazole resistant *C. glabrata* isolates when compared to susceptible isolates. [32]

An alternative mechanism of resistance to azoles that has been described in *C. glabrata* is the loss of mitochondrial function, also known as the petite phenotype [12, 33, 34] which is caused by a mutation in the mitochondrial DNA, resulting in the formation of petite cells that are unable to undergo aerobic respiration and that are therefore unable to use ethanol or glycerol as sole sources of carbon and energy. The exposure of C. glabrata cells to antifungals such as azoles has been appointed as an inducer of mtDNA damage, probably due to the direct binding of these antifungals to the mitochondrial DNA or because of an over-accumulation of reactive oxygen species (ROS) resultant from the impairment of mitochondrial function. Curiously, the expression of ABC transporters CgCdr1 and CgPdh1 was shown to be up-regulated in petite mutants, which may confer resistance to these pharmacological inhibitors by their increased efflux from the cell. [12, 34] Although no alteration in *ERG11* expression or its sequence have been identified, it was observed that petite mutants contain only small amounts of the intermediates from the ergosterol biosynthesis pathway but possess a disproportionate amount of ergosterol. [12] Nevertheless, it is important to note that the role of the petite mutant phenotype in the acquisition of resistance to azoles is not yet fully understood, given that in some studies [35] these mutants revealed an increased susceptibility to some azoles.

1.4.1. The CgPdr1 network and its involvement in azole resistance in *C. glabrata*

As previously mentioned, in *C. glabrata* the up-regulation of genes encoding the ABC-transporters *CgCDR1*, *CgPDH1* and *CgSNQ2* plays a relevant role for azole resistance in this species. [36-38] The transcriptional activation of these genes was found to be mediated by a single Zn(2)-Cys(6) transcription factor – CgPdr1p – an homologue of *S. cerevisiae* Pdr1p/Pdr3p. Consistently, elimination of *CgPDR1* was found to increase *C. glabrata* susceptibility to various azoles and the complementation of the deleted gene fully restores azole resistance of the mutant strains. [39] CgPdr1p was shown to act by binding to specific sequences – PDREs (pleiotropic drug response elements) – present in the promoter region of *CgCDR1*, *CgPDH1* and *CgSQN2*, thereby promoting

their up-regulation. *CgPDR1* also contains a PDRE in its promoter suggesting that auto-regulation of its transcription occurs. [40]

Extensive transcriptomic profiling revealed that CgPdr1 regulates a large number of genes in *C. glabrata*, besides those encoding drug-efflux pumps. Specifically, it was found that CgPdr1 regulates the expression of genes involved in lipid, fatty acid and sterols metabolism, in stress response, in transcriptional regulation and in adhesion, among other cellular functions. [12, 33, 40, 41] The family of proteins to which CgPdr1 belongs to – the zinc-finger protein family – is one of the largest families of transcriptional regulators known in eukaryotes displaying variable secondary structures and enormous functional diversity. [42] All the members of this protein family harbor the zinc finger motif which consists of one helix and a pair of antiparallel β strands, to which one or more zinc atoms are bound by cysteine or histidine residues. This binding stabilizes the domain and contributes to proper protein structure and function. [43] The majority of zinc finger proteins bind to DNA, thereby playing important roles in transcriptional and translational processes. Three functional domains are identified in Zn-finger proteins: the DNA binding domain (DBD), the regulatory domain (RD), and the acidic region (Figure 1.3). In addition, the DBD is compartmentalized into sub-regions – the zinc finger, the linker, and the dimerization domain – which contribute to DNA-binding specificity and to protein-DNA and protein-protein interactions. [42] The regulatory domain contains an important region displaying lesser homology among most members within this protein class, and it is termed the middle homology region (MHR). Although not always present in all zinc cluster proteins, this region is thought to play a role in regulating the transcriptional activity of these factors, since in many cases, deletion of the region that bridges the DNA binding domain to the activation domain results in constitutive activity of the transcriptional activator. [42] The functional domains – DNA binding domain, the regulatory domain, the activation domain and the xenobiotic binding domain – predicted for CgPdr1 [39, 44] are represented in Figure 1.3.

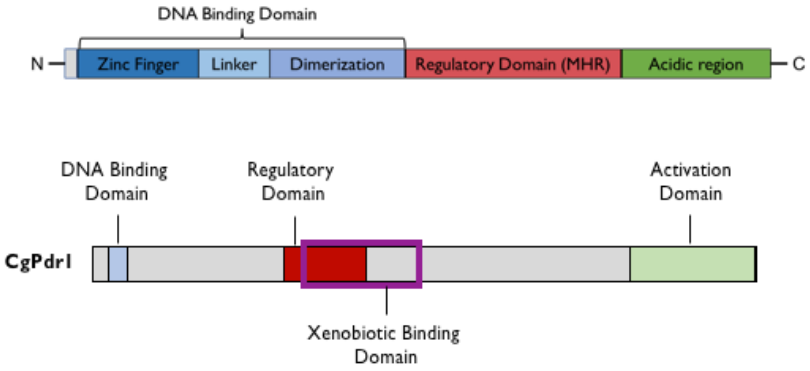

Figure 1.3 - Functional domains of zinc cluster proteins and of the CgPdr1 transcription factor.

The mechanism for activation of CgPdr1 as a response to exposure to azoles (Figure 1.4) was found to involve a specific domain – xenobiotic binding domain – of this transcription factor to which the antifungals are bound. For the time being, this mechanism has only been shown for ketoconazole. [44] Firstly, the antifungal drug binds directly to the xenobiotic binding domain (XBD) of the CgPdr1 transcription factor, which binds to the promoter sequence of drug-efflux genes. This promotes the binding of the Gal11p subunit of the Mediator complex through its KIX domain to the drug–Pdr1–DNA

complex. Gal11A is a component of the tail portion of the Mediator complex, which interacts with RNA polymerase II to regulate transcription, and it was identified as a co-activator for drug-dependent activation, interacting with Pdr1 through a binding domain that is similar to the KIX domain in humans. The mediator complex then facilitates recruitment of RNA polymerase II (Pol II complex), increasing the transcription of CgPdr1 target genes, including those encoding drug-efflux pumps. [44, 45] Notably, a molecule able to inhibit the interaction between the Gal11A KIX domain and Pdr1 was recently identified in a large scale high-throughput screening. [46] This compound, named iKIX1, prevented ketoconazole-induced upregulation of efflux pumps, as well as upregulation due to activating mutations in Pdr1, suggesting that it may be possible to overcome Pdr1-mediated azole resistance in *C. glabrata* by chemically interfering with Pdr1 activity. [46] To evaluate the therapeutic potential of iKIX1 and azole antifungal co-therapy, an established mouse model of disseminated fungal disease was used and in mice injected with an azole-resistant *C. glabrata* strain, only co-treatment with iKIX1 and fluconazole resulted in significant reductions in fungal burdens in the kidney and spleen. [46]

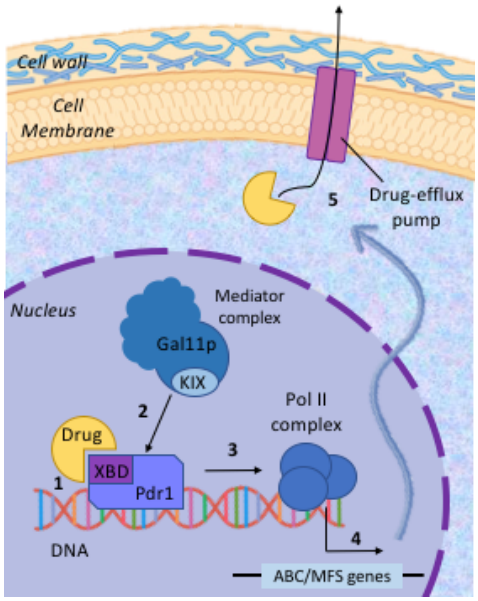

Figure 1.4 - Schematics depicting the activation of CgPdr1 in response to the exposure to drugs (adapted from Goffeau, 2008 [45]).

1.5. The acquisition of gain-of-function CgPdr1 mutations as a driver of *C. glabrata* resistance to azoles

The most frequently observed mechanism of resistance to azoles among *C. glabrata* strains involves the acquisition of activating mutations in the coding sequence of the *CgPDR1* gene that appear to result in the hyper-activation of the protein. Consequently, azole-resistant isolates expressing these gain-of-function CgPdr1 mutants are capable of a strong up-regulation of CgPdr1-target genes expression, including that of the drug efflux pumps *CgCDR1* and *CgPHD1*. [47] A wide range of GOF point mutations has been described to occur in the coding sequence of *CgPDR1*, a summary of them being shown in Figure 1.5. Several studies have demonstrated that the distribution of gain-of-function mutations in the *CgPDR1* gene is not associated with specific domains and these

can give origin to different transcription profiles by altering the overall structure of the transcriptional regulatory network of the strain. [27, 31, 39]

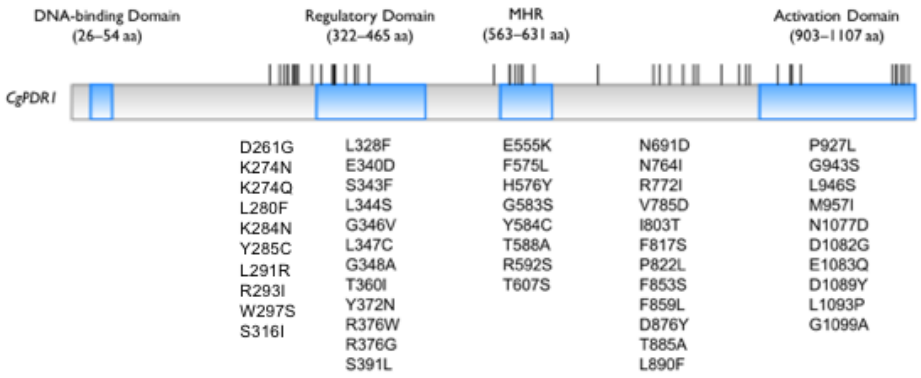

Figure 1.5 - Schematics compiling the *C. glabrata* PDR1 gain-of-function mutations described in Tsai *et al*., 2006 [33], Torelli *et al.*, 2008 [48], Ferrari *et al.*, 2009 [39], Berila *et al.*, 2009 [49], Tsai *et al.*, 2010 [27], Caudle *et al.*, 2011 [31] and Salazar *et al.*, 2017 [50]. The illustration of the CgPdr1 domains was done using the Illustrator for Biological Sequences online tool (available at http://ibs.biocuckoo.org/online.php).

In fact, a recent study [50] has highlighted the complexity of the regulatory mechanism associated with the transcriptional activity of CgPdr1. Salazar *et al.* demonstrated that the overlap between the genes regulated by the CgPdr1 GOF mutants K274N and K274Q was very limited (Figure 1.6.) revealing that even polymorphisms in the same CgPdr1 residue have a very different impact on the control of gene expression. One of the mechanisms that has been hypothesized to explain this divergence in the set of genes regulated by different CgPdr1 mutants is that they might be differently activated thereby resulting in a different interaction with the transcriptional machinery. [51]

Khakhina *et al.* [52] also furthered our understanding of the intricate regulation exerted by CgPdr1 and of the existing dissimilarities between the gain-of-function and wild-type variants of this protein. In this work, it was demonstrated that GOF Pdr1 derivatives present a higher increase in synthesis at the protein level than the wild-type protein, however the degradation of these mutant proteins was also enhanced indicating that they are less stable than the wild-type Pdr1. [52] Additionally, the overproduction of wild-type Pdr1 increased the expression of target genes such as *CgCDR1* but to a lesser extent than GOF derivatives did. Furthermore, site-directed mutagenesis of Pdr1 binding sites in the PDR1 promoter provided a clear demonstration that autoregulation of *CgPDR1* is required for its normal function. [52] Finally, Khakhina *et al.* discovered that the central domain of Pdr1 (corresponding to the amino acid sequence between residues 255-968) is critical to restrain its activity under normal conditions, given that the removal of this central domain produces a CgPdr1 derivative so transcriptionally active that it is not tolerated by the cell. [52]

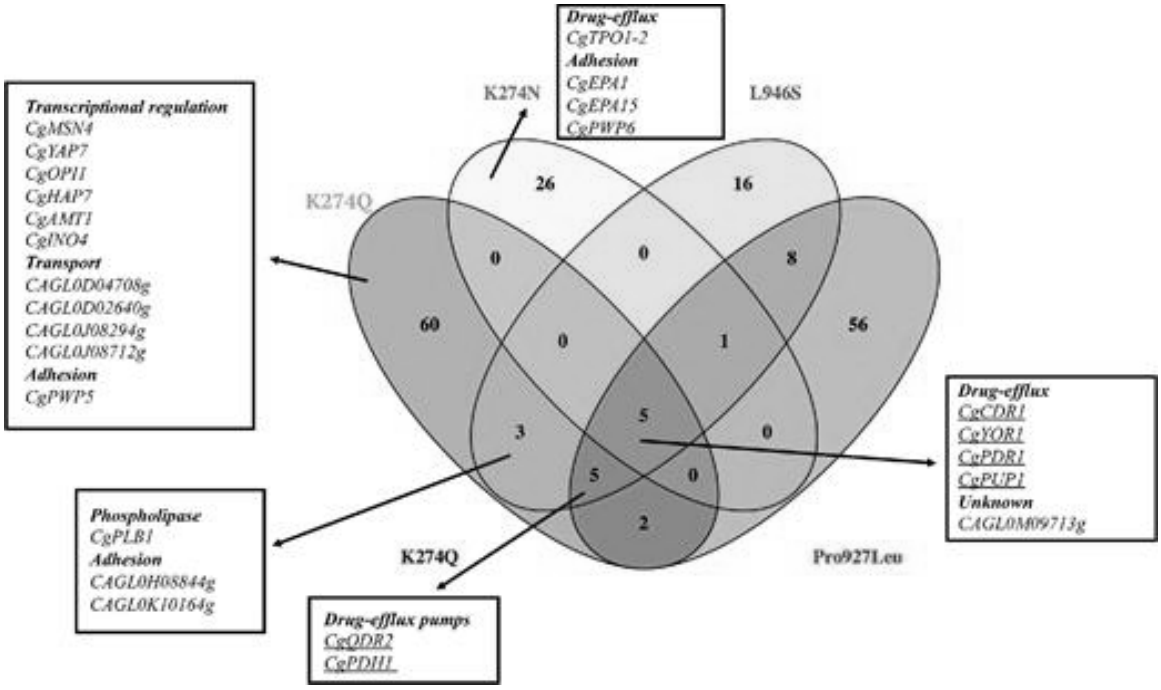

Figure 1.6 - Venn diagram comparing the set of genes regulated by the CgPdr1 GOF mutants K274Q, K274N, P927L and L946S, as revealed by transcriptomic analyses (retrieved from Salazar *et al.*, 2017 [50]). From the analysis of overlaps between GOF mutants it is possible to conclude that different amino acid substitutions clearly generate distinct transcriptomic responses.

1.6. Novel antifungal therapies

In spite of the advances in therapies over the last years, the development of antifungal drugs has always lagged behind fungal infections incidence, and most of these compounds have limited potential as systemic agents due to issues of toxicity, adverse effects or restricted bioavailability. Moreover, as highlighted before, their historic long-term application has generated the phenomenon of antifungal resistance, especially in what concerns azoles, which is still of major concern in clinical practice. Thus, the search for novel antifungal therapies, ideally inhibiting targets different from those that are inhibited by the currently used molecules, has become a pressing issue. [53]

Novel antifungal compounds can be discovered by slight alterations to already existing clinically used compounds, for example, newer formulations of amphotericin B, such as the lipid-associated and liposomal formulations, have demonstrated more selective fungal targeting and less host toxicity. [54] Alternatively, new antifungals can be obtained through the isolation and testing of completely new compounds from various sources. [53]

Several alternatives to current antifungals used in clinical practice have been developed recently and their descriptions and mode of action can be found summarized in Table 1.1. Since this thesis was focused on the exploration of the Ag(I)-camphorimine compounds, the following lines are dedicated to a slightly more elucidative description of what is known in this field concerning the antimicrobial, and more specifically the anti-*Candida*, effect of these molecules.

Silver has been known for its antimicrobial activity since the times of ancient Greece and silver nitrate has been in use for the treatment of burns and chronic wounds in clinical practice for a long

time now. [55] Nonetheless, after penicillin was introduced as a medical drug in the 1940s, the use of silver for the treatment of bacterial infections decreased and the grand antibiotic potential of this compound was left uncovered. [55] In the present scenario, silver nanoparticles as well as various silver-based compounds containing ionic silver (Ag^+) or metallic silver (Ag^0) exhibiting antimicrobial activity have been synthesized as an attempt to strike back against antifungal resistance.

Taking advantage of the interesting properties of silver-based compounds in what concerns their antimicrobial effects, recently J.M.S. Cardoso *et al.* (2017) focused on the synthesis and evaluation of the antibacterial and antifungal properties of silver camphorimine complexes obtained from silver nitrate and camphor derivatives. [56] In what concerns the antifungal activity of the Ag(I)-derived compounds tested (Figure 1.7.), Cardoso *et al.* verified that the complexes displayed a degree of efficacy towards the tested *Candida* species ranging from non-active (compound 4) to highly active (compound 2). Consistent with the observed increased resilience of *C. glabrata* species to antimicrobials, the MIC values of all Ag(I) complexes obtained for this species were higher than those obtained for *C. tropicalis* or *C. parapsilosis* (Figure 1.7.).

Compound	*C. albicans*	*C. glabrata*	*C. tropicalis*	*C. parapsilosis*
1	> 1000	31.3	3.9	> 1000
2	> 1000	15.6	7.8	2.0
3	> 1000	62.5	31.3	15.6
4	> 1000	> 1000	> 1000	> 500
5	> 1000	125	3.9	2.0
6	> 1000	62.5	7.8	2.0
7	> 1000	31.3	3.9	2.0
8	> 1000	62.5	7.8	2.0
$AgNO_3$	> 1000	15.6	3.9	2.0

Figure 1.7 – MIC values (μg/mL) for Ag(I) camphor complexes 1–8 and for $AgNO_3$ against *C. albicans, C. glabrata, C. tropicalis* and *C. parapsilosis*, based on the EUCAST microdilution method (retrieved from Cardoso *et al*., 2017 [56]).

Within the range of concentrations tested, none of the Ag(I) camphorimine complexes, nor $AgNO_3$, showed efficacy in inhibiting growth of *C. albicans* and this was attributed to the ability of this species to mediate reduction of silver present in the compounds leading to the formation of silver nanoparticles, which are far less toxic than the Ag(I)-derived compounds. [56] Nevertheless, the great majority of the compounds tested proved efficient in inhibiting the growth of *Candida glabrata*. [56] More recently, it was also shown that the efficacy of these Ag(I)-derived chemicals can be significantly increased when the tests are performed at a neutral pH. [57] Although further studies are required to fully understand the mechanisms underlying the specificity of the inhibitory effects exerted by Ag(I) complexes on the growth of *Candida* spp., the fact that these complexes efficiently inhibited the growth of NCAC species, with *C. glabrata* among them, can be considered promising as it constitutes a step forward in the development of novel antifungals alternative to azoles. [56]

Table 1.1 - Alternatives to current antifungals used in clinical practice developed over the last years along with their descriptions and mode of action.

Novel therapy	Description	Mode of action	Reference
Silver nanoparticles	Clusters of silver atoms in the size range of 1–100 nm, which can present numerous shapes	Not fully described. Possible disruption of membrane potential, leading to the leakage of cell constituents	Panáček *et al.* (2006) [58] Rai *et al*. (2009) [55] Panáček *et al.* (2009) [59] Kim *et al.* (2009) [60] Monteiro *et al.* (2011) [61]
Silver-camphorimine complexes	Complexes obtained from silver nitrate and camphor derivatives	Not fully described. Different targets and/or mechanisms of action in prokaryotic and eukaryotic cells	Cardoso *et al.* (2017) [56]
Biphosphinic cyclopalladated compounds	Palladium (II) complexed with a biphosphinic group	Not fully described. Inhibition of hyphae/pseudohyphae and biofilms	Muñoz *et al.* (2017) [62]
Polyoxometalates (POMs)	Transitional metal oxygen anion clusters	Inhibition of ergosterol biosynthesis, resulting in damage to the fungal cell membrane	Li *et al.* (2017) [63]
Antimicrobial Peptides (AMPs)	Small (<10 kDa) cationic and amphipathic peptides of variable length, sequence and structure natural synthesized by most living organisms as a defense against invading pathogens	Selective disruption of the plasma membrane and formation of ion channels, ultimately leading to the leakage of K^+ and other cellular components and to the lysis of the cell	Reddy *et al.* (2004) [64] Tam *et al.* (2015) [65]

1.7. Introduction to the theme of the thesis

This thesis goal was to continue fostering the work of the group in the identification of hyper-activating mutations in the coding sequence of the *CgPDR1* regulator in *Candida glabrata*, while simultaneously contributing for the understanding of how these modifications affect the overall biochemical activity of the protein. In this sense, the sequence of *CgPDR1* in a cohort of *C. glabrata* clinical isolates resistant to fluconazole and voriconazole was obtained and the influence of a set of SNPs, presumed to be gain-of-function mutations, in the resistance phenotype was investigated. This work was also aimed at obtaining further information on how the K274Q modification, recently disclosed as a new gain-of-function mutation in CgPdr1 [50], could affect the biochemical activity of CgPdr1 and, more specifically, its ability to bind DNA and recruit transcriptional machinery.

In a second line of work, to better understand how Ag(I)-camphorimine complexes inhibit growth of *Candida glabrata*, a transcriptomics approach based on species-specific DNA microarrays was used. More specifically, it was assessed how *C. glabrata* cells respond to a toxic, but not lethal, concentration of the Ag(I)-derived compound A. This compound has the chemical formula $\{Ag(NO_3)(^{III}L)\}n$, in which ^{III}L represents the ligand 3 which is camphorimine-based (Figure 1.8.). Despite its high anti-*C. glabrata* potential, compound A was found to exhibit a high toxicity against mammalian cell lines (results not published), therefore a set of other compounds – B and C – obtained with a different chemical synthesis route without including nitrate in their composition were produced. The chemical formulas of compounds B and C are, respectively, $\{Ag(CCA\text{-}Li)_2(CCA)\}$ and $\{Ag_2(CCA)_2(CCA\text{-}Li)\}$. Thus, the activities of compounds B and C, both having the ligand 1 in their chemical structures (Figure 1.8.), were tested against the reference strain *C. glabrata* CBS138 and against a cohort of azole-resistant strains.

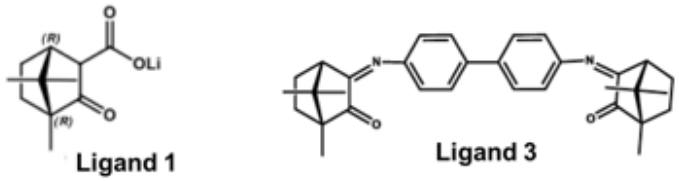

Figure 1.8 - Camphorimine complexes used as ligands of the compounds tested in this thesis. Ligand 1 is made up of camphor and lithium and it was used in the synthesis of compounds B and C. Ligand 3 is a camphor di-imine and was used to synthesize compound A.

2. Materials and Methods

2.1. Strains and growth media

The reference strain *Candida glabrata* CBS138 and a cohort of 10 *C. glabrata* clinical isolates (Annex A) were used in this experimental work. Besides these clinical isolates, a set of laboratory strains were also used as described in Table 2.1. An *Escherichia coli* DH5α strain was used as host for molecular biology procedures.

Table 2.1 - Description of the group of strains used in this work.

Strain	Genotype/Description	Origin
Candida parapsilosis ATCC 22019	*C. parapsilosis* laboratory strain	CEB (Minho)
S. cerevisiae BY4741	MATa his3Δ1 leu2Δ0 met15Δ0 ura3Δ0	Euroscarf
S. cerevisiae BY4741 Δpdr1	MATa his3Δ1 leu2Δ0 met15Δ0 ura3Δ0 YGL013c::kanMX4	Euroscarf
C. glabrata Cg66032	Cg66032 Δura3	Katiyar *et al.*, 2006 [66]
C. glabrata SKY107	Δhis3::FRT Δtrp1::FRT Δleu2::FRT Δura3::tn903 Δpdr1::natMX4	Khakhina *et al.*, 2018 [52]

C. glabrata cells were batch-cultured at 30ºC, with orbital agitation (250 rpm) in rich growth medium Yeast Peptone Dextrose (YPD) or RPMI (Roswell Park Memorial Institute Medium). YPD medium contains, per liter, 20 g glucose (Merck Millipore), 10 g yeast extract (HiMedia Laboratories, Mumbai, India) and 20 g Peptone (HiMedia Laboratories). RPMI medium contains, per liter, 20,8 g RPMI-1640 synthetic medium (Sigma), 36 g glucose (Merck Millipore), 0,3 g of L-glutamine (Sigma) and 69 g of MOPS (3-(Nmorpholino) propanesulfonic acid, Sigma). The various *C. glabrata* strains were maintained at -80ºC in YPD medium supplemented with 86% glycerol (v/v) (Merck). All media were prepared using deionized water. YPD medium was sterilized by autoclave for 15 minutes at 121ºC and 1 atm. RPMI medium was filtered with a 0,22 µm pore size filter or using a filtration system and 0,2 µm white membrane filters (Whatman), and preserved at 4ºC until further use. Unless otherwise stated, the pH of the RPMI growth medium was adjusted to 7 using NaOH as the alkalinizing agent. *E. coli* DH5α strain was maintained and cultivated in LB medium (Sigma) or in this same medium supplemented with 1:10 of ampicillin.

2.2. Preparation of Ag(I)-derived chemicals

The stock solutions of Ag(I)-derived compounds were prepared from the powder, supplied by Professor Fernanda Carvalho (DEQIST), using DMSO (Dimethyl sulfoxide, Sigma) or ethanol 70% as the solvent, depending on the compound in question. The concentrations tested for each compound in this study ranged from 0,977 mg/L to 500 mg/L.

2.3. Yeast genomic DNA extraction

Yeast genomic DNA was extracted from *C. glabrata* or *S. cerevisiae* colonies by harvesting three loops of biomass to a 1,5 mL Eppendorf tube, containing approximately 100 µL of glass beads (0,5 mm) and 200 µL lysis buffer (Tris 50 mM, EDTA 50 mM, NaCl 250 mM, SDS 0.3%). The tubes were vortexed for 2 minutes at maximum speed and then incubated at 65ºC for 1 hour. Afterwards, the tubes were chilled on ice for 2 minutes and then a second round of vortexing was performed. The obtained disrupted cell suspension was centrifuged at 13000 rpm for 15 minutes at 4ºC and the supernatant was transferred to a clean Eppendorf. Next, 20 µL of NaAC 3M (pH 4,8) and 400 µL of absolute ethanol were added to the suspensions to induce DNA precipitation. The samples were then kept for, at least, 30 minutes at -20ºC and centrifuged at 13000 rpm, during 20 minutes at 4ºC. The pellet obtained was washed with 500 µL of ethanol 70%, and then centrifuged at 13000 rpm for 8 minutes at 4ºC. Finally, the supernatant was discarded and the pellet obtained was dried in speed vacuum and ressuspended in 30 µL of deionized water.

2.4. Cloning of various CgPdr1 constructs to assess their biochemical activity

To clone several CgPdr1 constructs – DBD, DBD+GOFs, DBD+GOFs+RD and DBD+RD – a strategy based on cloning by ligation was used. Firstly, the DNA fragments corresponding to each construct were amplified by PCR, using DNA extracted from *C. glabrata* CBS138 as template, primers that generated overhangs containing restriction sites recognized by the enzymes BamHI and ClaI (Table 2.2) and the Phusion High-Fidelity DNA Polymerase (Thermo Scientific). The DBD+RD construct was generated by overlapping PCR, which consisted of 3 separate PCR amplifications: the first using primers FW_BamHI and RV_OP, the second using primers FW_OP and RV_RD_NarI and the last one using primers FW_BamHI and RV_RD_NarI. The reaction mixtures and the experimental conditions used are described in Tables 2.3 and 2.4.

Table 2.2 - Primers used for the amplification of the DNA correspondent to each CgPdr1 construction. The underlined nucleotides correspond to the sequence that will allow digestion with the restriction enzyme indicated in the primer ID. The nucleotides marked in bold will allow the obtainment of the DBD+RD construct by overlapping PCR.

Primer ID	Sequence (5'-3')
FW_BamHI	CGCGGATCCATGCAAACATTAGAAACTACATC
FW_OP	**ATCATATTACATCTAGAC**GATTTAGTCTTGCAGAATCTTT
RV_DBD_ClaI	CCATCGATGATACTCTCCCTGTTGGT
RV_GOFs_ClaI	CCATCGATTGCAAGACTAAATCCACA
RV_RD_NarI	CATAGAGGCGCCCGCTCATAACAGAGTCAA
RV_OP	**GTCTAGATGTAATATGAT**AACTGGGTGCATTTTGAA

Then the amplified DNA fragments were digested with BamHI (Takara) and ClaI (Takara) or, in the case of the constructions including the regulatory domain, BamHI and NarI (New England Biolabs). The plasmid pYEF2-DBD_Haa1_VP16 [67] was then digested with BamHI and ClaI and the restriction product was run in an electrophoresis gel and purified. Subsequently, each construct was inserted into the pYEF2-DBD_Haa1_VP16 plasmid by ligation, using the T4 DNA ligase

(ThermoFisher) and the reaction mixture described in Table 2.5 which was incubated over-night at 16ºC. Afterwards, 5 µL of each ligation mixture containing each construct were used to transform *E. coli* DH5α cells according to the protocol described in subchapter 2.11.

Table 2.3 - PCR reaction mixture used amplify the CgPdr1 constructs.

Component	Volume per reaction
HF Buffer	5 µL
dNTPs (10mM)	0,5 µL
Primer FW (100 pmol/µL)	0,5 µL
Primer RV (100 pmol/µL)	0,5 µL
Template DNA (200 ng/µL)	1 µL
$MgCl_2$ (50 mM)	0,9 µL
DMSO	0,5 µL
Phusion (2 U/µL)	0,1 µL
ddH_2O	16 µL
TOTAL	25 µL

Table 2.4 - Conditions of the PCR cycles for amplification of the CgPdr1 constructs. The extension time was calculated using a calculus basis of 30 s per kilobase of the amplified fragment.

Temperature	Time	
98ºC	30 seconds	
98ºC	10 seconds	30 cycles
59ºC	20 seconds	
72ºC	30 s/ Kb	
72ºC	7 minutes	
4ºC	∞	

Table 2.5 – Reaction mixture used to insert each construct into the pYEF2-DBD_Haa1_VP16 plasmid.

Component	Amount per reaction
10x T4 DNA Ligase Buffer	4 µL
T4 DNA Ligase (5 U/µL)	1 µL
Insert DNA	300 ng
Plasmid DNA	100 ng
ddH_2O	Remaining volume
TOTAL	20 µL

Plasmid DNA was extracted from the positive candidates using the NZYMiniprep Kit (NZYTech) and integration was confirmed by analyzing the restriction map of the recovered plasmids with the restriction enzymes BamHI and ClaI. After integration was confirmed, the sequences inserted were verified by Sanger sequencing as a paid service from STABVIDA.

2.5. Microdilution assays

To assess resistance levels to the compounds B and C, the *C. glabrata* CBS138 reference strain, 6 of the *C. glabrata* fluconazole-resistant isolates described in Annex A (FFUL412, FFUL443, FFUL674, FFUL830, FFUL886 and FFUL887) and a *C. parapsilosis* ATCC 22019 strain were used.

The microdilution methodology followed is summarized in Figure 2.1. For each microdilution assay, the wells of two 96 multiwell-plates were filled with 100 µl of RPMI, being that one of the plates was filled with RPMI at pH 5 and the other one with RPMI at pH 7. Columns 1 to 10 of each plate were used to test the selected compound as well as ethanol alone to verify if it had any effect on cellular growth that could mislead the results obtained. The day before this assay, *Candida* strains were inoculated separately in 5 mL of YPD medium and grown for 18 hours at 30ºC and 250 rpm. Each compound tested was first dissolved in 70% ethanol, since dilution in DMSO proved inefficient for these substances, being that the ethanol volume (in µL) used in dilution was equal to 30 times the mass (in mg) of the compound used. Serial 1:2 dilutions were then made, starting by taking 100 µL of column 10 and adding them to well 9, and so on and so forth, until column 1 from which the 100 µL added should be removed after thorough up-and-down mixing. In column 11 of the plate (control), cells were diluted in 100 µL of sterile drug-free medium and in column 12 (blank) only the sterile drug-free growth medium was added. The volume of inoculum added to each well was calculated to achieve an initial optical density (OD_{600nm}) of 0,05. After inoculation, the 96-multiwell plates were incubated without agitation at 37°C for 24h. Finally, the cells were ressuspended and the OD_{600nm} was read in a SPECTROstar^{nano} microplate reader (BMG Labtech).

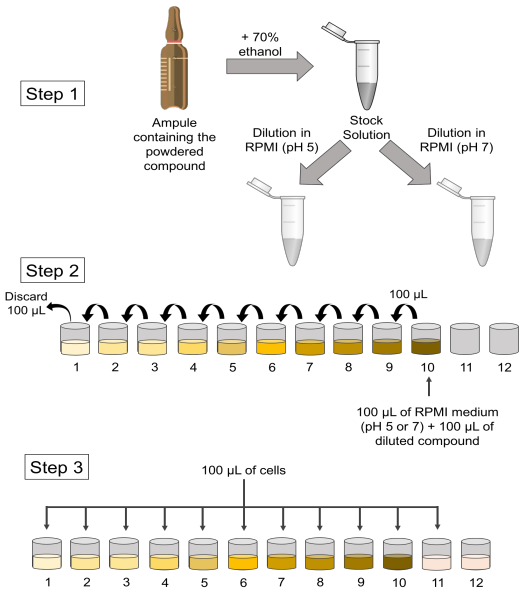

Figure 2.1 – Microdilution methodology used in this work.

2.6. Growth curves in the presence of the Ag(I)-derived chemicals

Growth of the *C. glabrata* CBS138 strain in RPMI growth medium (pH 7) in the presence of inhibitory concentrations of compound A was accompanied during 12 hours in 250 mL Erlenmeyer flasks. Firstly, CBS138 cells were inoculated in 5 mL of YPD and grown over-night at 30ºC with 250 rpm agitation. Two Erlenmeyer flasks were prepared with 100 mL of RPMI medium (pH 7) and to one of them a certain volume of compound A was added in order to obtain a final concentration of 15,63 mg/L and the same volume of DMSO (control) was added to the other flask. After this, the optical density (OD_{600nm}) of the cultures grown over-night was measured and calculations were done in order to determine the inoculum volume to be added to the two flasks to obtain an initial OD_{600nm} of 0,2. Finally, the two inoculated flasks (test and control) were incubated at 30ºC with orbital agitation (250 rpm) and samples were taken hourly to measure optical density and accompany cellular growth.

2.7. RNA extraction and microarrays

Firstly, CBS138 cells were inoculated in 5 mL of YPD and grown over-night at 30ºC with 250 rpm agitation. Six Erlenmeyer flasks were prepared with 150 mL of RPMI medium (pH 7) and to three of them a certain volume of compound A was added in order to obtain a final concentration of 15,63 mg/L and the same volume of DMSO (control) was added to the remaining three flasks. After this, the

optical density (OD_{600nm}) of the cultures grown over-night was measured and calculations were done in order to determine the inoculum volume to be added to the flasks to obtain an initial OD_{600nm} of 0,2. The calculated volumes were filtered using a filtration vacuum system and the paper filters were then placed inside the respective flasks which were incubated at 30ºC with orbital agitation (250 rpm) for one hour. After this time, 100 mL were collected from each flask and placed in centrifuge tubes whilst the remaining 50 mL were incubated at 30ºC with orbital agitation (250 rpm) and samples were taken hourly to measure optical density and accompany cellular growth. The 100 mL of cells from each of the six samples were centrifuged for 7 minutes at 7000 rpm and 4ºC and the pellets were ressuspended in 1 mL of the supernatant. From now on the cells were kept on ice whenever possible. The ressuspended pellets were centrifuged for 2 minutes at 2000 rpm on a tabletop centrifuge and the supernatants were removed. Finally, the pellets were preserved at -80ºC. RNAs were extracted using RiboPure™-Yeast Kit (life technologies) and their concentration and purity were quantified using Nanodrop Spectrophotometer ND-1000 (Alfagene). Microarray analysis was performed at iBIMED (University of Aveiro) using the Two-Color Microarray-Based Gene Expression Analysis Kit from Agilent and following the protocol associated to this kit which consisted of the following main steps: (1) labeling the control and test samples with Cyanine 3-CTP and Cyanine 5-CTP, respectively; (2) purifying and quantifying the labeled RNAs; (3) hybridization reaction with the gasket slides containing the species-specific DNA microarray; (4) microarray slides washing; (5) scanning and feature extraction.

2.8. Assessment of gene expression based on real time RT-PCR

The expression of *CgCDR1* and *CgPUP1* genes was compared in 8 azole-resistant *C. glabrata* isolates – FFUL29, FFUL56, FFUL412, FFUL443, FFUL607, FFUL674, FFUL830 and FFUL866 – by real time RT-PCR. In order to do so, the strains were pre-inoculated in 25 mL of YPD and incubated at 30ºC with orbital agitation (250 rpm) for 8 hours. Afterwards, the strains were inoculated in 100 mL of RPMI following the calculations illustrated by Equations 2.1, 2.2 and 2.3 and incubated at 30ºC and 250 rpm.

$$x = \frac{expected\ incubation\ time}{duplication\ time} \qquad \textbf{Equation 2.1.}$$

$$OD_{initial} = \frac{0{,}8}{2^x} \qquad \textbf{Equation 2.2.}$$

$$V_{initial} = \frac{OD_{initial} \times V_{RPMI}}{OD_{measured\ in\ pre-inoculum} \times Dilution\ Factor} \qquad \textbf{Equation 2.3.}$$

When the OD_{600nm} of the cultures achieved approximately 0,2 (corresponding to mid-exponential phase), cells were harvested by centrifugation for 7 minutes, at 4°C and 7000 rpm using a Beckman J2-MC Centrifuge and the pellets were frozen at -80ºC until further use. RNA extraction was performed using the phenol method described in chapter 2.9 of this section. Conversion of total RNA

into cDNA was performed in a C1000 Thermal Cycler (Bio-Rad), using the TaqMan® Reverse Transcription Kit (Applied Biosystems) and the experimental conditions used are presented in Tables 2.6 and 2.7.

Table 2.6 - PCR reaction mixture used for each strain in order to obtain cDNA.

Component	Amount per reaction
10X RT Buffer	1 µL
$MgCl_2$ (25 mM)	2,2 µL
ddNTPs (2,5 mM)	2 µL
Random Hexamers (50 µM)	0,5 µL
RNase Inhibitor (20U/µL)	0,2 µL
MultiScribe™ Reverse Transcriptase (50U/µL)	0,25 µL
Template DNA	1 µg
Water	x µL
TOTAL	10 µL

Table 2.7 - Conditions of the PCR cycles for obtainment of cDNA.

Temperature	Time
25ºC	10 minutes
48ºC	30 minutes
95ºC	5 minutes
4ºC	∞

The subsequent quantitative PCR step was performed using the reaction mixture represented in Table 2.8 and a 7500 Real Time PCR System (Applied Biosystems) and respective software. The sequences of the primers used for each gene tested are listed in Table 2.9. Gene expression was calculated using gene *RDN25* as an internal control.

Table 2.8 - RT-PCR reaction mixture.

Component	Volume per reaction
SYBR® Green super mix (BioRad)	12,5 µL
Primer FW (4 pmol/µL)	2,5 µL
Primer RV (4 pmol/µL)	2,5 µL
cDNA	2,5 µL
Water	5 µL
TOTAL	25 µL

Table 2.9 - Sequences of the primers used to perform RT-PCR.

Primer ID		Sequence (5'-3')
CgCDR1	FW	GCT TGC CCG CAC ATT GA
	RV	CCT CAG GCA GAG TGT GTT CTT TC
CgPUP1	FW	CAC TGG TGC GCT GAA AGG TG
	RV	TGT CCC AGG CTA TCT TTG CC

2.9. RNA extraction (phenol method)

Firstly, the cell pellets stored at -80ºC were thawed on ice, ressuspended in 900 µl of AE buffer (50 mM AcLi, 10 Mm EDTA, pH 5,3, 0,1% DEPC) and then 90 µl of 10% SDS were added. The tubes were vortexed for 5 minutes and then 800 µl of phenol (Sigma) were added for RNA purification. The tubes were vortexed for 5 seconds and incubated at 65°C for 4 minutes. After this incubation, the tubes were immediately placed in a dry ice mixture until phenol crystals appeared (approximately 8 minutes). Following this, a centrifugation was performed for 5 minutes at 15000 rpm and 4°C and the upper phases formed were transferred to new eppendorf tubes. Subsequently, 400 µL of phenol and 400 µL of a chloroform: isoamyl alcohol solution (24:1 ratio) were added to each eppendorf tube, the tubes were vortexed for 5 seconds and centrifuged at 15000 rpm, 4°C for 5 minutes and the upper phases formed were transferred to new eppendorf tubes. The previous step was repeated. Afterwards, 800 µL of the chloroform: isoamyl alcohol solution was added to the tubes, which were then centrifuged at 15000 rpm, 4°C for 5 minutes and the upper phases formed were transferred to new eppendorf tubes. Next, 90 µl of sodium acetate (3 M) and 1 mL of 100% cold ethanol were added to the tubes, which were then shaken in the vortex and stored at -20°C for at least 20 minutes. Then the tubes were centrifuged for 20 minutes at 15000 rpm and 4°C, the supernatants were discarded and the precipitates were washed with 750 µL of 70% cold ethanol and centrifuged for 15 minutes, 15000 rpm at 4°C. The supernatants were removed with the assistance of a syringe and the pellets were dried in speed-vac for 15 minutes, 45ºC in V-AL mode. Finally, the dried pellets were ressuspended in 50 µL of ddH_2O treated with 0,1% DEPC and the concentration of RNA samples was measured in Nanodrop Spectrophotometer ND-1000 (Alfagene).

2.10. Site-directed Mutagenesis

Firstly, eight specific mutagenesis primers were designed (Table 2.10) to introduce four distinct mutations into the *PDR1* gene of *C. glabrata*. These mutations were E5K, R35K, K274Q and I392M, which were identified in azole-resistant isolates FFUL674, FFUL866, FFUL887 and FFUL443, respectively.

Table 2.10 - Sequences of the primers used for site-directed mutagenesis.

Primer ID	Sequence (5'- 3')
E5K_FW	GTT ATT GAG AGA ATA TGC AAA CAT TAA AAA CTA CAT CAA AAT CAA ATC CAG G
E5K_RV	CCT GGA TTT GAT TTT GAT GTA GTT TTT AAT GTT TGC ATA TTC TCT CAA TAA C
K274Q_FW	AAG ATT AAT GAA AGT GCC ACC ACT CAG TCA CTT GAA ACA AAC TTG
K274Q_RV	CAA GTT TGT TTC AAG TGA CTG AGT GGT GGC ACT TTC ATT AAT CTT
I392M_FW	ATA TCA ATG AAG AGT CGA TAT CGA TGG CCA ACC CGT TAG
I392M_RV	CTA ACG GGT TGG CCA TCG ATA TCG ACT CTT CAT TGA TAT
R35K_FW	CAA AAG TTG GAA AAG CTT GTG ATA GCT GTA AAA GGA GGA AAA TAA AA
R35K_RV	TTT TAT TTT CCT CCT TTT ACA GCT ATC ACA AGC TTT TCC AAC TTT TG

Next, the amino acid substitutions previously mentioned were introduced into the *CgPDR1* gene through PCR amplification using the pSP76 vector previously extracted from an *E. coli* DH5α strain as

the template DNA, the PfuTurbo DNA polymerase kit (Agilent) and with the specific primers listed in Table 2.10. The reaction mixture and the experimental conditions used are described in Tables 2.11 and 2.12.

Table 2.11 - PCR reaction mixture used in order to obtain the desired mutations.

Component	Volume per reaction
10x Reaction Buffer	5 µL
dNTPs (10 mM)	1 µL
Primers (10 pmol/µL)	1 µL
Template DNA (50 ng/µL)	0,5 µL
PfuTurbo DNA polymerase (2,5 U/µL)	1 µL
Water	40 µL
TOTAL	50 µL

Table 2.12 - Conditions of the PCR cycles for site-directed mutagenesis.

Temperature	Time	
95ºC	30 seconds	
95ºC	30 seconds	16 cycles
55ºC	1 minute	
68ºC	9 minutes	
68ºC	7 minutes	
4ºC	∞	

After the PCR was concluded, 1 µL of DpnI (New England BioLabs) was added to each reaction mixture and then the PCR tubes were incubated at 37ºC for 1 hour. Following the incubation period, 5 µL of the digested PCR products correspondent to each mutation were used to transform *E. coli* DH5α competent cells, using the protocol described in chapter 2.11 of this section, and the DNA of the obtained candidates was extracted using NZYMiniprep Kit (NZYTech), quantified and sent for Sanger sequencing using the primers listed in Table 2.13. The sequencing reaction was performed by STABVIDA as a paid service.

Table 2.13 - Primer sequences used to amplify the selected regions of *CgPDR1* gene containing the desired mutations.

Primer ID	Sequence (5'- 3')
FW1_CgPDR1	ATG CAA ACA TTA GAA ACT ACA TCA AAA TCA
REV4_CgPDR1	CAC ACT AAG ATC CAT TGG CTT TTG AAT

After confirming the presence of the mutations designed, the pSP76 vectors containing each mutation in *CgPDR1* were used to transform the following strains using the Alkali-Cation TM Yeast Transformation Kit (MP Biomedicals) and following the protocol associated to it: *S. cerevisiae* BY4741, *S. cerevisiae* BY4741 Δ*pdr1*, *C. glabrata* Cg66032 and *C. glabrata* SKY107.

2.11. Classical Transformation of *E. coli* DH5α competent cells

Firstly, the aliquots containing 50 µL of *E. coli* DH5α competent cells, which were stored at -80ºC, were thawed on ice. Subsequently, 5 µL of the insert were added to each chilled tube containing 50 µL of competent cells, which were then incubated for 30 minutes on ice. Then, the cells were subjected to heat-shock by incubation at 42ºC for 45 seconds followed by a 2-minute incubation on

ice. Following this, 200 µL of LB medium were added to the cells, which were then incubated with orbital agitation (250 rpm) at 37ºC for 1 hour. During this incubation, plates containing solid LB medium supplemented with ampicillin were warmed at 37ºC. After the incubation was complete, the cells were subjected to centrifugation at 8000 rpm, for 3 minutes in a tabletop centrifuge and the supernatants were discarded. Finally, the pellets were ressuspended in 100 µL of LB medium, plated in LB solid medium supplemented with ampicillin and incubated at 37ºC for 24 hours.

2.12. Sanger sequencing of *CgPDR1* gene of azole-resistant isolates

The sequence of the *CgPDR1* gene of 4 different *C. glabrata* isolates – FFUL29, FFUL56, FFUL 556 and FFUL607 – was obtained by primer walking. To do so, 4 rounds of PCR were performed for each strain using specific primers whose sequence is indicated in Table 2.14.

Table 2.14 - Sequences of the primers used to sequence the *CgPDR1* of isolates FFUL29, FFUL56, FFUL556 and FFUL607.

Primer ID	Sequence (5'- 3')
FW1_CgPDR1	CTT CCA TTA CTT CGT ACC C
FW2_CgPDR1	GCC TAG TAC AAG AAG AAC AAA AGT TG
FW3_CgPDR1	TCC ATT GAC GCC ATT GAG TTA CAA C
FW4_CgPDR1	TTACGACCGCAATTTGGACTCAGAGG
REV4_CgPDR1	CACACTAAGATCCATTGGCTTTTGAAT
REV3_CgPDR1	CAG AGT GCC AAA GTA TGC AGC CTT
REV2_CgPDR1	CGG CGA GGG TAA ATT CAA CTG ATA C
REV1_CgPDR1	GAC AGT GTG CAT AGC CTG

The PCR amplification was performed using the reaction mixture and the experimental conditions described in Tables 2.3 and 2.4. The sequencing reaction was performed by STABVIDA as a paid service. Clustal Omega was used for sequence alignment establishing as a reference for the comparative analysis the sequence of *CgPDR1* from the reference strain *C. glabrata* CBS138, susceptible to azoles.

2.13. Growth curves in the presence of Fluconazole

Growth curves of the transformants obtained in subchapter 2.10 in the presence of fluconazole concentrations ranging between 0,25 – 128 mg/L were performed using essentially the same experimental setup described above for the microdilution method. Growth, taken as the increase in OD_{600nm} of the culture, was monitored for 84 hours with 6 hour intervals between each time-point. Each experiment was performed in triplicate.

3. Results and Discussion

3.1. Unveiling novel gain-of-function mutations in *CgPDR1*

Following the results obtained in previous works [50, 57] which led to the identification of new gain-of-function (GOF) mutations in the *CgPDR1* gene from *C. glabrata*, it was hypothesized if a new group of isolates phenotyped [50] as fluconazole- and/or voriconazole-resistant – FFUL29, FFUL56, FFUL556 and FFUL607 – could also encode CgPdr1 gain-of-function mutants. For the isolates FFUL412, FFUL443, FFUL674, FFUL830 and FFUL866, the sequence of *CgPDR1* had been obtained in a prior work [57] revealing a set of non-synonymous substitutions that can be found summarized in Table 3.1. Subsequently, the *CgPDR1* gene sequences from isolates FFUL29, FFUL56, FFUL556, and FFUL607 were obtained by Sanger sequencing. The alignment of the sequences obtained for each one of these four isolates with the sequence of the azole-susceptible CBS138 strain is shown in Annexes B, C, D and E, and the set of mutations exhibited by them is represented in Table 3.1.

Table 3.1 - Alterations in the amino acid sequence of CgPdr1 transcription factor encoded by the azole-resistant isolates when compared to the CgPdr1 encoded by the CBS138 strain. The non-synonymous SNPs associated with a resistance phenotype were marked in red, the susceptible non-synonymous SNPs were marked in green and the non-described non-synonymous SNPs were marked in blue. The candidates to be new GOF variants of CgPdr1 were marked with an asterisk (*).The described mutations were retrieved from Ferrari *et al*., 2009 [39], Caudle *et al*., 2011 [31], Katiyar *et al.*, 2016 [68], and Salazar *et al.*, 2017 [50].

		5	10	35	91	98	143	173	243	274	376	392	555	558
Previous Works	CBS138	E	S	R	V	L	T	D	D	K	R	I	E	G
	FFUL412			P	I	S	P					M*		
	FFUL443			P	I	S	P					M*		
	FFUL674	K*			I	S			N					
	FFUL830		T		I				N				K	
	FFUL866			K*	I	S			N					
	FFUL887					S			N	Q				
In this Work	FFUL29				I	S			N					
	FFUL56				I	S			N					C*
	FFUL556				I	S			N		W			
	FFUL607				I	S			N		W			

The non-synonymous SNPs V91I, L98S and D243N had been previously described in isolates both resistant and susceptible to azoles [39], hence they were not considered as drivers of the resistance phenotype exhibited by the strains and hence were discarded as putative CgPdr1 GOFs. Mutations K274Q, R376W and E555K were already described [39, 50] as GOF mutations and could therefore underlie the voriconazole and fluconazole-resistance phenotype of the FFUL556, FFUL607, FFUL830 and FFUL887 isolates. The G558C replacement found in the *CgPDR1* sequence of isolate FFUL56 was only recently identified in other azole-resistant strains but its relevance as a GOF variant

of CgPdr1 remains to be confirmed. [68] However, since FFUL56 displayed no other mutations associated with azole resistance, it was possible that this mutation could be responsible for the azole-resistance observed in this clinical isolate, possibly constituting a new *CgPDR1* GOF. The non-synonymous SNPs E5K, R35K and I392M, were not yet described and were hypothesized to represent new gain-of-function mutations of this regulator considering the azole-resistance phenotype exhibited by isolates harboring these different alleles (FFUL412, FFUL443, FFUL674 and FFUL866). Interestingly, the coding sequence of the *CgPDR1* allele encoded by the fluconazole- and voriconazole-resistant isolate FFUL29 had no replacement that could be linked with the azole-resistance phenotype of the strain, thereby suggesting that this phenotype could be driven by changes in other genes/proteins. In this sense, genomic DNA of this isolate was extracted and sent for whole-genome sequencing. However, during the time of this thesis this analysis had not yet been completed and therefore no results concerning this matter can be discussed.

As said above, the results obtained sustain the idea that the non-synonymous E5K, R35K, I392M and G558C SNPs are candidates to lead to hyper-activation of CgPdr1. To test this hypothesis, the expression of two genes – *CgCDR1* and *CgPUP1* – found to be up-regulated in a wide set of GOF CgPdr1 mutants [47], was monitored in isolates FFUL412, FFUL443, FFUL56, FFUL674 and FFUL866, in comparison with the transcript levels observed in the reference strain CBS138. The expression of *CgCDR1* and *CgPUP1* was also monitored in isolate FFUL29 and also in isolates FFUL607 and FFUL830, these last two serving as positive controls since they harbor already-known GOF variants of CgPdr1. In case the E5K, R35K, I392M and G558C mutations do lead to a constitutive activation of CgPdr1 (and are, consequently, GOF variants of this regulator) an up-regulation of target genes in these isolates would be expected even during growth in the absence of azole stress.

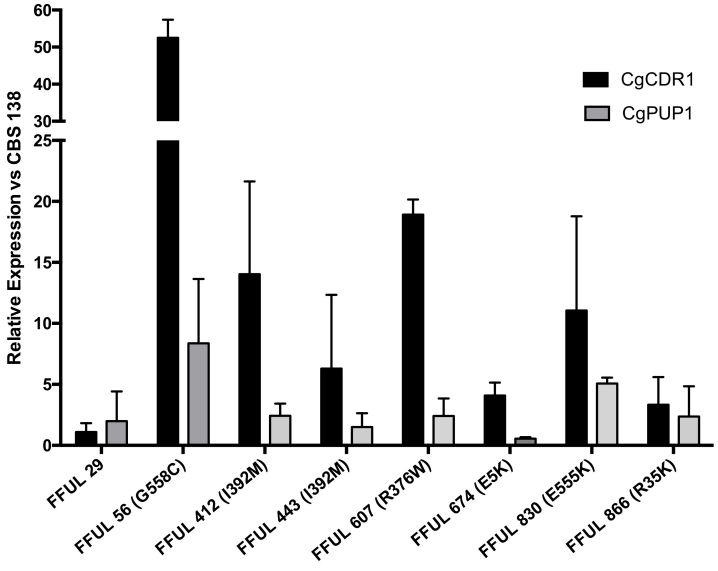

Figure 3.1 - Comparison of the transcript levels of *CgCDR1* and *CgPUP1* genes in various azole-resistant isolates. Cells of the different isolates were cultivated in RPMI growth medium until mid-exponential phase, after which the expression of *CgCDR1* and *CgPUP1* genes was compared by qRT-PCR. The values represented for each isolate are relative to the value obtained for the CBS138 strain, which was considered to be equal to 1. Gene expression was calculated using *RDN25* as an internal control.

As expected, up-regulation of *CgCDR1* and *CgPUP1* in isolates FFUL607 and FFUL830 (used as positive controls) was observed (Figure 3.1.). A clear up-regulation of these two genes was also observed in isolate FFUL56, supporting the idea that the G558C substitution could be a novel gain-of-function variant of CgPdr1 (Figure 3.1.). As previously observed [39, 48], CgPdr1 target genes are not always coordinately expressed in azole-resistant isolates, most likely due to differences in their promoter sequences or by differences in the transcriptional capacity of CgPdr1p. Regarding isolates FFUL412 and FFUL443, which harbor the I392M variation, there was a considerable up-regulation of *CgCDR1* in FFUL412 which was less noticeable in FFUL443. Nevertheless, in both cases, up-regulation of *CgPUP1* was observed of about 2-fold. As for isolate FFUL866, which harbors the R35K variant, the result was also not very clear since the transcript levels of *CgPUP1* and *CgCDR1* were only slightly above (around 2-fold) those observed for the reference strain CBS138 (Figure 3.1.). Interestingly, in isolate FFUL29 the expression of both *CgPDR1* and *CgPUP1* was identical to the one observed for the CBS138 strain, reinforcing the idea that the resistance phenotype of this isolate could be the result of a CgPdr1-independent molecular mechanism.

In conclusion, profiling of *CgCDR1* and *CgPUP1* in the fluconazole- and voriconazole-resistant isolates clearly suggest that the G558C substitution represents a new gain-of-function mutation in CgPdr1. Taking a significant upregulation as a threshold of two-fold expression difference [39], the replacements E5K (identified in isolate FFUL674), R35K (identified in isolate FFUL866) and I392M (identified in isolates FFUL412 and FFUL443), were also considered as potential GOF variants of CgPdr1.

3.2. Assessing the role of candidate CgPdr1 GOF mutations in the azole-resistance phenotype of *C. glabrata* and *S. cerevisiae*

To evaluate the potential of the amino acid substitutions identified in subchapter 3.1. as candidates to be novel gain-of-function variants of *CgPDR1* it was decided to examine their effect in the azole-resistance phenotype of a known susceptible strain. As such, a strategy was devised aiming to engineer the E5K, R35K and I392M substitutions in the coding sequence of the *CgPDR1* gene (using site-directed mutagenesis) cloned in the plasmid pSP76 [52] together with its endogenous promoter and terminator regions (Figure 3.2.). As a positive control it was also engineered the replacement K274Q, recently described [50] as a new CgPdr1 GOF variant. Site-directed mutagenesis was performed using primers specifically designed for each amino acid substitution. After confirming the engineering of the selected substitutions by Sanger sequencing, the pSP76 vector driving the expression of wild-type *CgPDR1* or the mutated vector driving the expression of the E5K, R35K, I392M or K274Q variants were transformed in *S. cerevisiae* BY4741, in *S.*

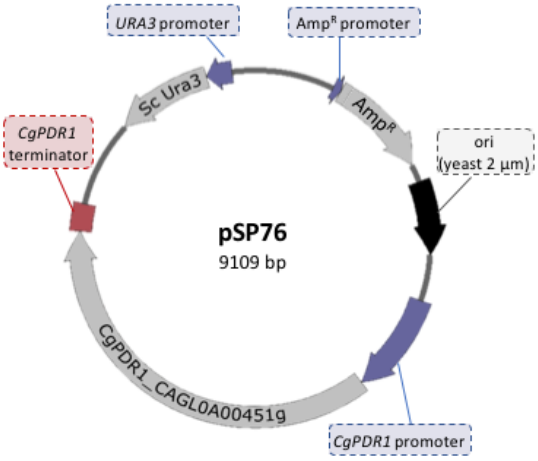

Figure 3.2 – Map depicting the features of plasmid pSP76.

cerevisiae BY4741 Δ*pdr1* mutant, in *C. glabrata* Cg66032 (wild-type) and *C. glabrata* SKY107 *(*Δ*pdr1* mutant). The resulting transformants are listed in Annex F. Afterwards, tolerance of the different strains to increasing concentrations of fluconazole, ranging from 0,25 to 128 mg/L, was tested giving rise to the results that are shown in Figures 3.3 and 3.4.

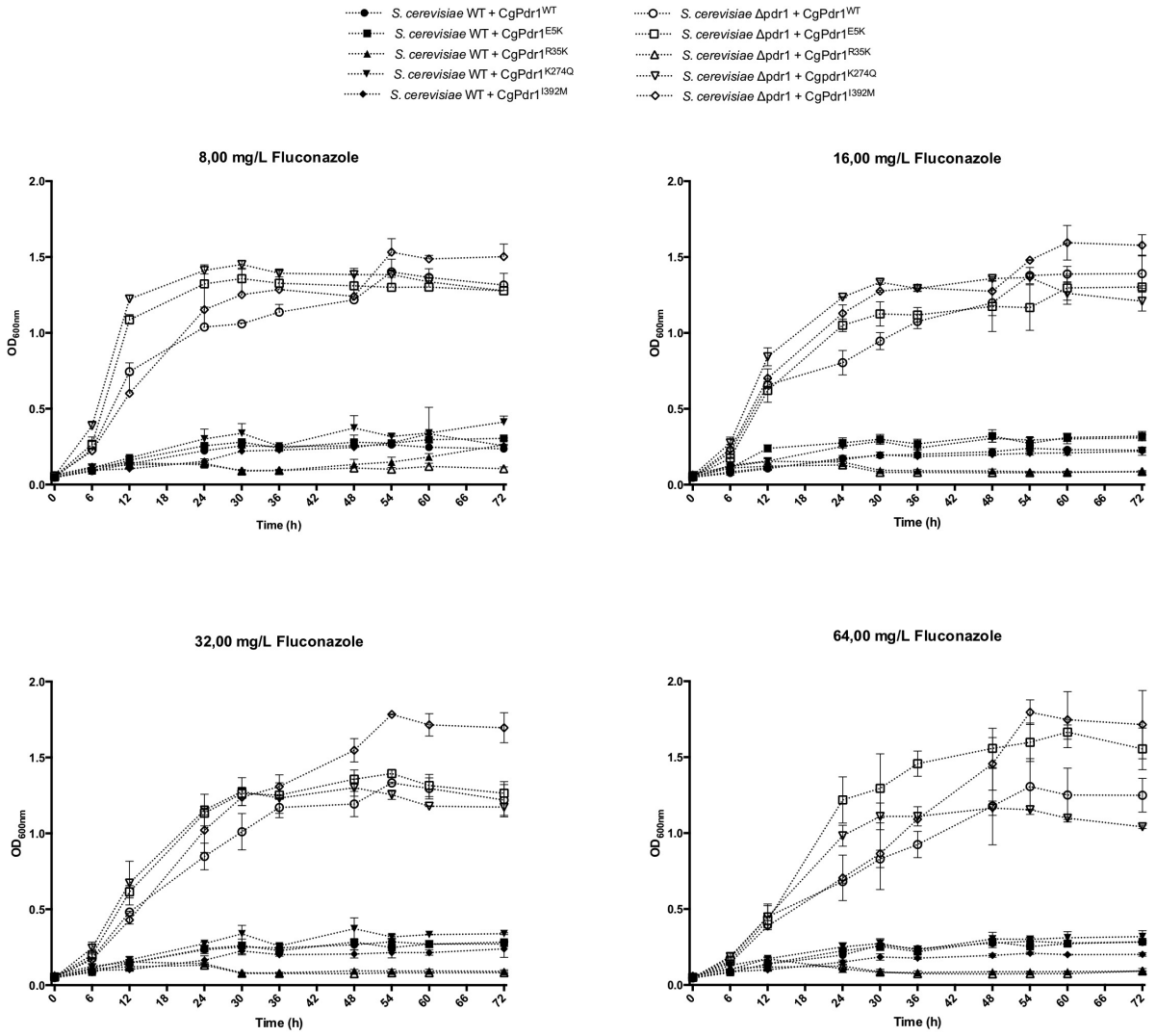

Figure 3.3 - Growth curves of the various *S. cerevisiae* wild-type and Δ*pdr1* mutant transformants when in presence of fluconazole concentrations ranging between 8,00 – 64,00 mg/L.

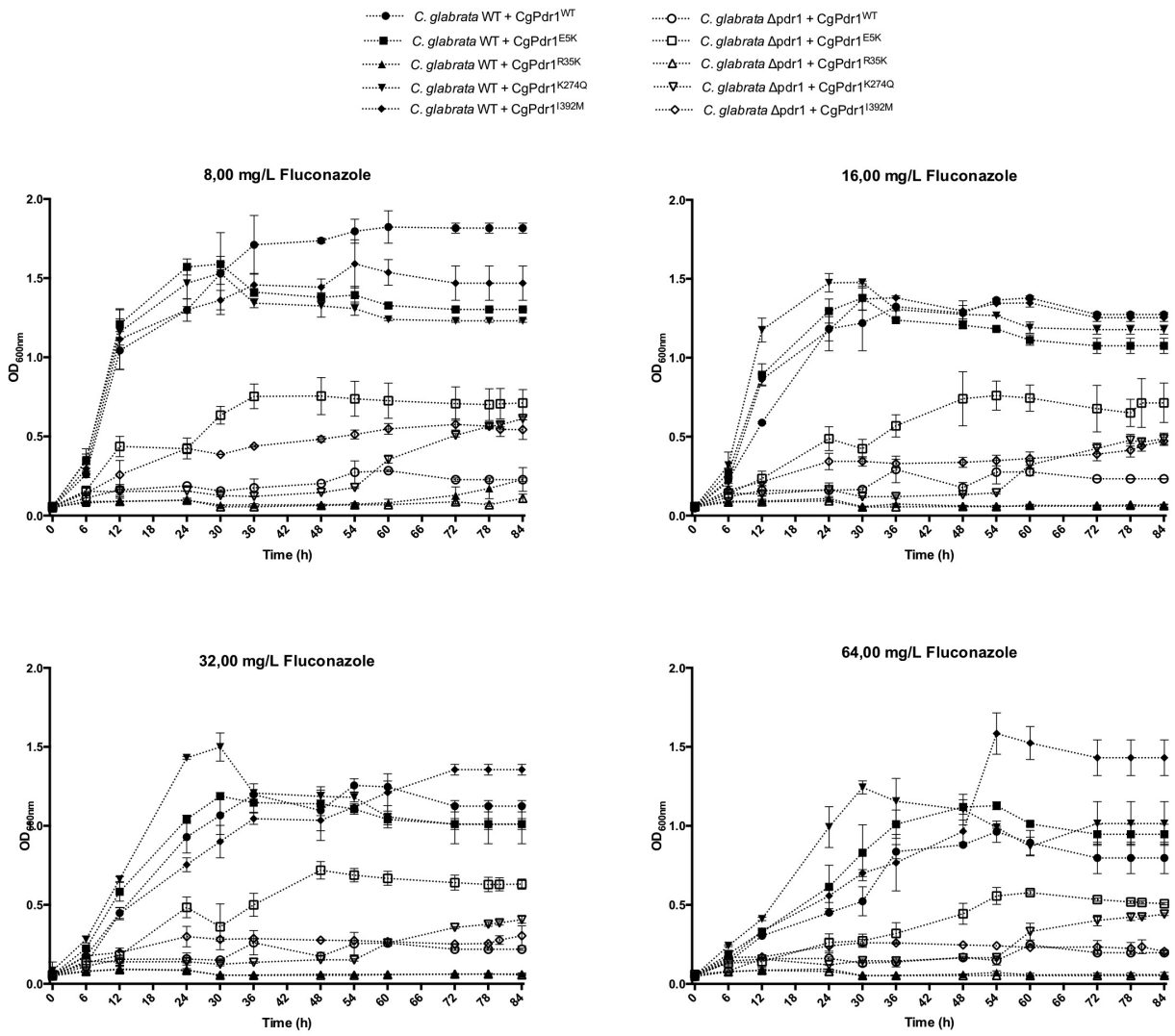

Figure 3.4 - Growth curves of the various *C. glabrata* wild-type and Δ*pdr1* mutant transformants when in presence of fluconazole concentrations ranging between 8,00 – 64,00 mg/L.

In the absence of fluconazole, all the *S. cerevisiae* and *C. glabrata* transformants based on the wild-type or *Δpdr1* mutant backgrounds were able to grow, albeit the growth rate of transformants based on *C. glabrata Δpdr1* or *S. cerevisiae* wild-type cells was considerably lower, especially for those cells transformed with the *CgPDR1*^{R35K} allele (see Annex G).

In the presence of fluconazole, the reduced fitness of *S. cerevisiae* wild-type cells transformed with the different *CgPDR1* alleles was clearly evident, given that none of these transformants was able to grow even when exposed to only 8 mg/L of fluconazole (Figure 3.3). The expression of the *CgPDR1* gene in a background that already expresses the endogenous *ScPDR1* and also its orthologue *ScPDR3* seems to result in deleterious effects for the *S. cerevisiae* cells. In fact, the burden of replicating extra chromosomes has been previously described as fitness-reducing in *S. cerevisiae* [69] and aneuploidy in this yeast has been shown to generally reduce growth both in rich medium and in stressful conditions. [70] In the Δ*pdr1* mutant background no significant deleterious effect of expressing *CgPDR1* was observed and complementation of the *ScPDR1* deletion was verified (Figure 3.3).

Notably, Δ*pdr1* cells transformed with the E5K, K274Q or I392M CgPdr1 variant alleles displayed a remarkably higher growth (around 5-fold higher) than cells transformed with the wild-type *CgPDR1* allele (Figure 3.3). In the case of Δ*pdr1* cells transformed with the *CgPDR1*^{R35K} allele, no significant growth was observed (Figure 3.3) and the reduced fitness of these cells was also observed in control conditions (Annex G). It is difficult at this point to understand why the expression of this *CgPDR1*^{R35K} allele would be prejudicial for cell fitness in a Δ*pdr1* background (which does not express Pdr1 and thus one cannot argue that it could result from burden of over-expressing the protein) and even in conditions where the protein is expected to be inactive, such as control conditions. Transformation of *C. glabrata* wild-type and Δ*pdr1* cells with this *CgPDR1*^{R35K} allele also resulted in a lower fitness, either in the presence or absence of fluconazole (Figure 3.4 and Annex G). It can be hypothesized that the R35K substitution can result in a highly hyperactive form of CgPdr1 that would result in toxicity for the *S. cerevisiae* and *C. glabrata* cells, something that has been observed recently for a form of CgPdr1 not having an inhibitory domain. [52] Constitutively active transcription factors (TFs) may reduce the fitness of the cells even under nonselective by limiting their adaptive flexibility thus representing an unnecessary waste of energy and resources [71] Notably, the isolate from which this CgPdr1 allele was recovered exhibited a considerably lower fitness than the remaining isolates (results not shown).

Transformation of *C. glabrata* wild-type cells with the plasmid driving the expression of *CgPDR1*^{WT} did not affect cellular growth, contrary to what was observed in *S. cerevisiae*, with the exception of the cells transformed with the *CgPDR1*^{R35K} allele, as discussed above (Figure 3.4). For higher concentrations of fluconazole (64 mg/L) it was noticeable the robust growth exhibited by cells transformed with the *CgPDR1*^{I392M} allele and, less significantly, with the *CgPDR1*^{E5K} and *CgPDR1*^{K274Q} alleles (Figure 3.4). A generalized reduction of fitness was observed in all transformants based on the Δ*pdr1* mutant background and this was verified both in the presence and absence of fluconazole (Figure 3.4 and Annex G). Despite this, it was clearly visible the more prominent growth of Δ*pdr1* cells transformed with the *CgPDR1*^{E5K} allele and also, less significantly, with the *CgPDR1*^{K274Q} allele (Figure 3.4). Overall, the results obtained both in *S. cerevisiae* and in *C. glabrata* strongly support the K274Q (this being in line with previous results from our lab [50]), the E5K and the I392M amino acid substitutions as new gain-of-function mutations in CgPdr1.

3.3. Unraveling the role of GOF mutations in the biochemical activity of CgPdr1

To assess the effect of CgPdr1 amino acid substitutions over the biochemical activity of this transcription factor, first their effect in the transactivation potential of the regulator was tested. To do so, several variants of CgPdr1 were constructed and a cloning strategy based on plasmid pYEF2-DBD_Haa1-VP16 [67] which takes advantage of the heterologous transactivation domain VP16 was devised (Figure 3.5 A). A schematic representation of the various constructs proposed is shown in Figure 3.5 B. These constructs aimed to make different combinations of the DNA binding domain (DBD), the region upstream of the regulatory domain where a great number of GOF mutations have been identified [27, 31, 39, 50] (GOFs region) and the regulatory domain (RD) of CgPdr1.

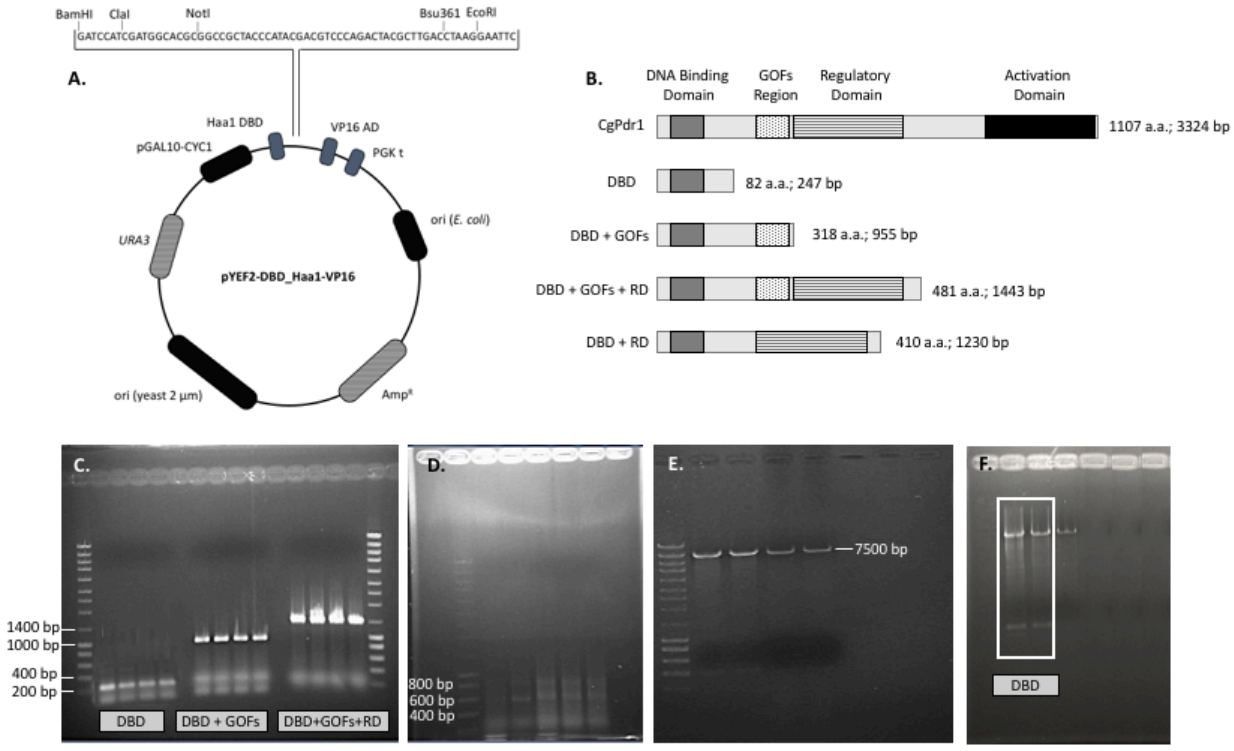

Figure 3.5 - A) Schematics depicting the features of vector pYEF2-DBD_Haa1_VP16; B) Structural domains of the CgPdr1 transcription factor and the various protein constructs elaborated to assess its biochemical activity; C) PCR amplification to obtain the fragments corresponding to three CgPdr1 constructs: DBD, DBD+GOFs and DBD+GOFs+RD; D) PCR amplification to obtain the fragments corresponding to the two segments of the DBD+RD construct; E) Gel electrophoresis depicting the pYEF2-DBD_Haa1_VP16 digested with BamHI and ClaI; F) Restriction digest of the DNA extracted from candidates containing the DBD construct with BamHI and ClaI.

The first step consisted in the PCR amplification of the DNA fragments corresponding to each construct (Figure 3.5 C and D), using primers that generated overhangs containing restriction sites recognized by the enzymes BamHI and ClaI. This amplification was successful for the DBD, DBD+GOFs and DBD+GOFs+RD constructs, as can be observed in the gel electrophoresis (Figure 3.5. C) by the presence of 247 bp, 955 bp and 1443 bp fragments, respectively. However, the DBD+RD construct was not fully obtained given that the two fragments constituting it – DBD (721 bp) and RD (510 bp) – were never successfully joined by overlapping PCR (Figure 3.5 D). Subsequently, the pYEF2-DBD_Haa1_VP16 plasmid was digested with BamHI and ClaI and the restriction product was run in an electrophoresis gel and purified to ensure that the BamHI-ClaI portion was indeed excised, preventing re-circularization. As can be seen in Figure 3.5 E, fragments of approximately 7500 bp were obtained, corresponding to the digested pYEF2-DBD_Haa1_VP16 plasmid. Afterwards, the DNA fragments corresponding to each construct were digested with the appropriate restriction enzymes and cloned by ligation using the previously digested pYEF2-DBD_Haa1_VP16 plasmid in *E. coli* DH5α. Up to now, the only two positive candidates obtained corresponded to the DBD construct (Figure 3.5. F) however, upon Sanger sequencing, it was verified that the DBD constructs inserted into the pYEF2-DBD_Haa1_VP16 plasmid contained several nucleotides misplaced hence not making it a viable option to assess the biochemical activity of this CgPdr1 domain alone.

3.4. Transcriptomic analysis of *C. glabrata* cells grown in the presence of the Ag(I)-derived compound A

In order to define the experimental setting to conduct the planned transcriptomic analysis, it was first necessary to assess the inhibitory effect of compound A on the growth of *C. glabrata* CBS138 strain in RPMI growth medium (at pH 7), since the previous works undertaken were not performed in planktonic conditions but in microplates. [57] Cultivation of *C. glabrata* cells in RPMI supplemented with 15,63 mg/L of compound A resulted in a lag phase of about 8 hours during which no significant growth was observed (Figure 3.6 A). After this period, cells resumed exponential growth at a growth rate of 0,09 h^{-1}, comparing with 0,19 h^{-1} registered in control conditions. A slight, but detectable, reduction in the number of CFUs in the Ag(I)-exposed populations (Figure 3.6. B) was also observed.

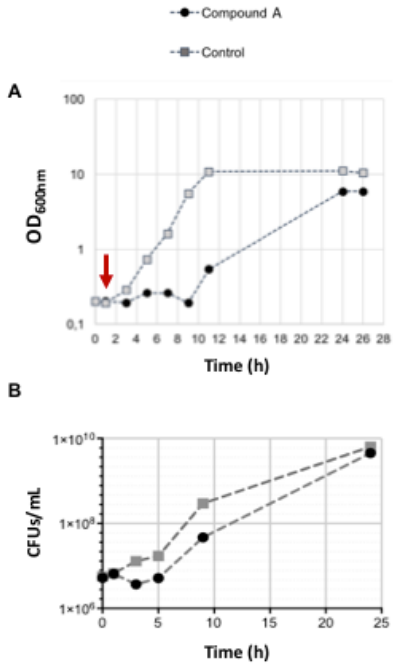

Figure 3.6 - A) Growth curves of *C. glabrata* CBS138 strain in the presence (•) and absence (■) of compound A. The red arrows mark the time-point (t=1 hour) selected to perform cell harvest for later RNA extraction. B) Colony forming units per milliliter calculated for each tested condition over a 24-hour period.

Based on the results obtained it was decided to examine how compound A would affect the genomic expression of *C. glabrata* CBS138 after 1 hour of exposure, a period corresponding to the early adaptation phase. After cell cultivation and RNA extraction, hybridization was performed using the species-specific Agilent microarrays, in collaboration with the group of Professor Manuel Santos from the University of Aveiro (iBiMED). The resulting data were processed using the BRB-ArrayTools program in association with Excel and the fold-changes were estimated utilizing Lowess smoothing. There were 225 up-regulated genes (fold-changes greater than or equal to 2) and 746 down-regulated genes (fold-changes lower than or equal to -2).

Afterwards, the up- and down-regulated genes were categorized using the MIPS Functional Catalogue Database tool [72] and the PathoYeastract *C. glabrata* database. [73] The outputs obtained were organized and summarized in Figure 3.7 and in Tables 3.2 and 3.3. Functional clustering (based

on MIPS Functional Catalogue) of the genes whose expression changed above the threshold of 2-fold used revealed an enrichment of those involved in: amino acid metabolism, nitrogen, sulfur and selenium metabolism, carbon and carbohydrate metabolism, secondary metabolism, glycolysis and gluconeogenesis, protein processing (proteolytic), protein/ peptide degradation, cytoplasmic/nuclear protein degradation and oxidative stress response. Functional clustering of the genes whose expression decreased below 2-fold upon exposure to compound A revealed an enrichment of those involved in: nucleotide/nucleoside metabolism, carbon and carbohydrate metabolism, cell cycle and DNA processing, RNA synthesis, siderophore-iron transport, sugar transport and disease, virulence and defense.

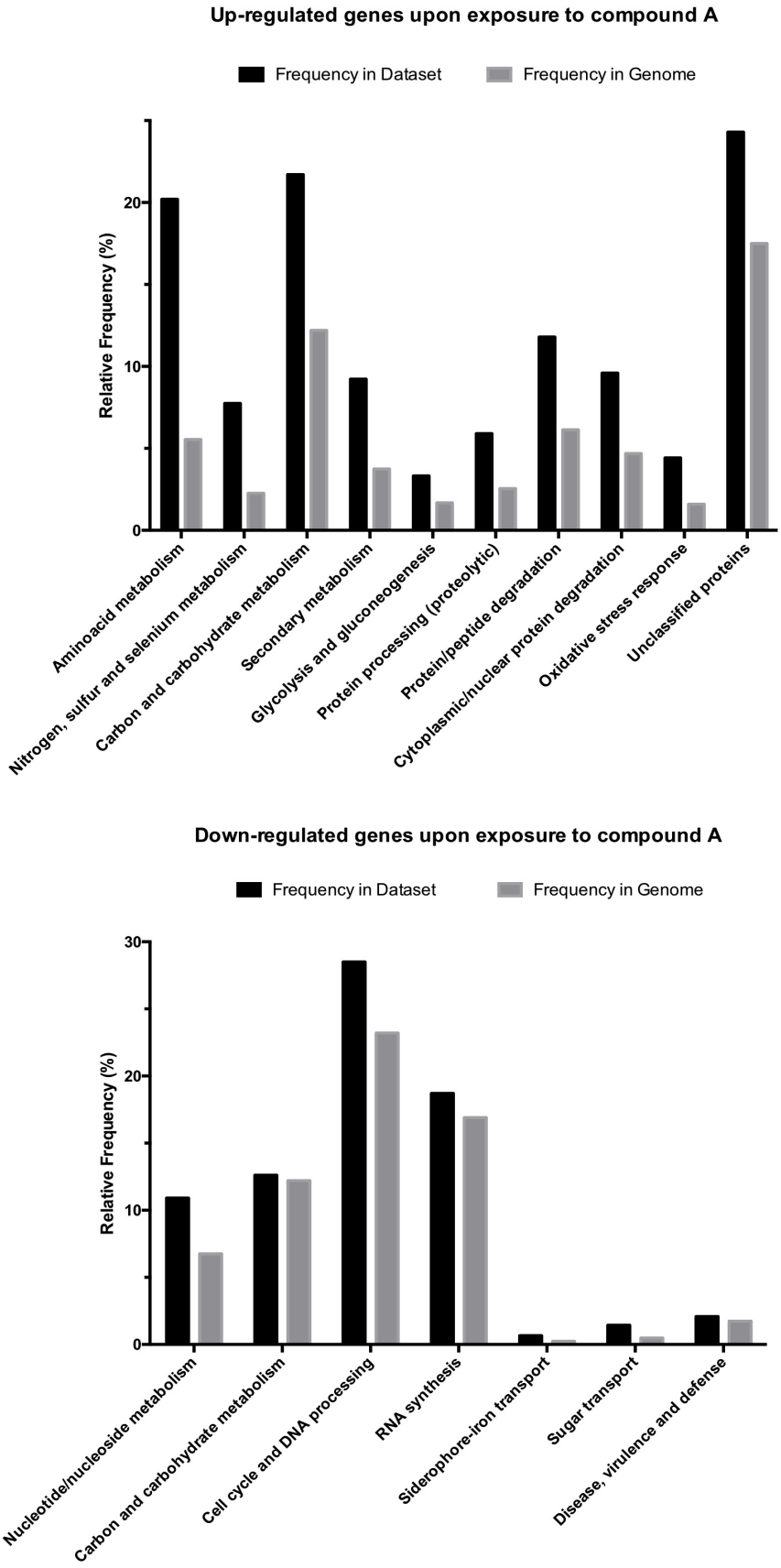

Figure 3.7 - Graphical representation of the relative frequency of the main biological functions found to be enriched in the set of genes up-regulated (up) or down-regulated (down) in *C. glabrata* cells upon exposure to compound A.

Table 3.2 - Main functional categories identified by the MIPS Functional Catalogue Database tool (p-value <0,05) as up-regulated in the presence of compound A, alongside with the major genes within each category, their fold-change when compared to the control condition, and their description as provided by PathoYEASTRACT.

Category	Gene code	Gene Name	Fold-change	Description
Amino acid Metabolism	CAGL0B03839g	MET3	8,92	Uncharacterized ORF; Orthologues have sulphate adenylyltransferase (ATP) activity
	CAGL0D06402g	MET15	9,80	O-acetyl homoserine sulfhydrylase, orthologue of S. cerevisiae MET17; required for utilization of inorganic sulphate as sulphur source
	CAGL0F07029g	MET13	94,59	Uncharacterized ORF; Orthologues have methylenetetrahydrofolate reductase (NAD(P)H) activity and role in methionine biosynthetic process
	CAGL0G01903g	MET1	18,73	Uncharacterized ORF; Orthologues have a role in cellular response to drug, methionine biosynthetic process, siroheme biosynthetic process
	CAGL0I04994g	MET6	5,28	Uncharacterized ORF; 5-methyltetrahydropteroyltriglutamate homocysteine methyltransferase
	CAGL0J03762g	MET7	13,53	Uncharacterized ORF; Orthologues have tetrahydrofolylpolyglutamate synthase activity
	CAGL0K08668g	MET28	56,98	Uncharacterized ORF; bZIP domain-containing protein
	CAGL0K06677g	MET8	34,83	Uncharacterized ORF; Putative bifunctional dehydrogenase and ferrochelatase;
	CAGL0B00902g	HIS4	4,09	Uncharacterized ORF; Phosphoribosyl-AMP cyclohydrolase; phosphoribosyl-ATP pyrophosphatase; histidinol dehydrogenase
	CAGL0L02937g	HIS3	4,45	Verified ORF; Putative imidazoleglycerol-phosphate dehydratase
	CAGL0L00759g	HIS1	2,37	Uncharacterized ORF; ATP phosphoribosyltransferase;
Protein/peptide Degradation	CAGL0E01793g	YPS6	4,65	Uncharacterized ORF; Putative aspartic protease; predicted GPI-anchor; member of a YPS gene cluster that is required for virulence in mice
	CAGL0E01419g	YPS2	7,99	
	CAGL0E01815g	YPS8	8,16	
	CAGL0E01771g	YPS5	6,83	
	CAGL0E01859g	YPS10	11,37	
	CAGL0E01881g	YPS11	9,01	
	CAGL0E01837g	YPS9	7,43	
	CAGL0M04191g	YPS1	6,33	Verified ORF; Yapsin family aspartic protease; predicted GPI-anchor;
Oxidative stress response	CAGL0K10868g	CTA1	2,57	Verified ORF; Putative catalase A; regulated by oxidative stress and glucose starvation
	CAGL0K00803g	TRX2	2,71	Uncharacterized ORF; Protein described as thioredoxin involved in oxidative stress response;
	CAGL0C01705g	GPX2	3,01	Uncharacterized ORF; Putative glutathione peroxidase

Table 3.3 - Main functional categories identified by the MIPS Functional Catalogue Database tool (p-value<0,05) as down-regulated in the presence of compound A, alongside with the major genes within each category, their fold-change when compared to the control condition, and their description as provided by PathoYEASTRACT.

Category	Gene code	Gene Name	Fold-change	Description
Siderophore-iron transport	CAGL0E04092g	SIT1	0,13	Verified ORF; Putative siderophore-iron transporter with 14 transmembrane domains required for iron-dependent survival in macrophages
	CAGL0F06413g	FET3	0,04	Uncharacterized ORF; Putative copper ferroxidase involved in iron uptake
	CAGL0H03487g	AFT1	0,31	Verified ORF; Putative RNA polymerase II transcription factor involved in regulation of iron acquisition genes; required for growth under iron depletion
	CAGL0I06743g	FTR1	0,05	Uncharacterized ORF; Putative ferrous iron transmembrane transporter involved in iron uptake
	CAGL0J07980g	CAGL0J07980g	0,27	Uncharacterized ORF; Orthologues have copper chaperone activity and role in cellular copper ion homeostasis, cellular iron ion homeostasis, cellular response to oxidative stress, copper ion transport, regulation of iron ion transmembrane transport
Sugar transport	CAGL0A01804g	HXT1	0,10	Uncharacterized ORF; Orthologues have fructose transmembrane transporter activity, pentose transmembrane transporter activity, role in glucose transmembrane transport, mannose transmembrane transport and plasma membrane localization
	CAGL0A02233g	HXT4/6/7	0,08	Uncharacterized ORF; Orthologues have glucose transmembrane transporter activity and plasma membrane localization
	CAGL0A02211g	HXT6/7	0,06	Uncharacterized ORF; Orthologues have glucose transmembrane transporter activity, pentose transmembrane transporter activity, role in glucose transmembrane transport and plasma membrane localization
	CAGL0A01782g	HXT4	0,08	Uncharacterized ORF; Orthologues have glucose transmembrane transporter activity, pentose transmembrane transporter activity and plasma membrane localization
	CAGL0A02321g	HXT3	0,21	Uncharacterized ORF; Orthologues have fructose transmembrane transporter activity, glucose transmembrane transporter activity, mannose transmembrane transporter activity and role in fructose import across plasma membrane, glucose import across plasma membrane
	CAGL0H09196g	VRG4	0,31	Verified ORF; GDP-mannose transporter involved in glycosylation in the Golgi

It was possible to conclude that the up-regulated functions in *C. glabrata* upon exposure to compound A with the highest relative frequency values in the dataset were amino acid metabolism, carbon metabolism and protein/peptide degradation. Carbon metabolism was not an unexpected response of yeast cells, given that these microorganisms are usually dependent of a carbon source in order to strive, even more so when exposed to an environmental stress such as compound A. Therefore, the over-expression of the group of genes involved in the oxidative stress response was further analyzed instead of carbon metabolism.

Regarding amino acid metabolism, genes related to the biosynthesis and degradation pathways of methionine and histidine were those found to be most activated within this functional class (Table 3.2). The over-expression of the *MET* and *HIS* genes could be hypothesized to result from the high affinity of silver, one of the constituents of compound A, for the sulfur existing in amino acids and peptides, which has been previously verified in a study [74] that assessed the affinity of silver and copper for the various existing amino acids. The results obtained by Lee *et al.* [74] listed methionine and histidine as two of the five amino acids to which silver had a higher affinity. If this is so, compound A could be able to sequester these amino acids, leading to a reduction in their cellular availability hence resulting in an over-expression of the genes involved in the biosynthesis of methionine and histidine.

A set of genes involved in oxidative stress response were also found to be up-regulated in compound A-exposed cells including: catalase A (CTA1), thioredoxin (TRX2) and glutathione peroxidase (GPX2) (Table 3.2). The antimicrobial activity of silver has been attributed to its interference with the activity of respiratory enzymes and components of the microbial electron transport system [75] and also its ability to bind glutathione leading to the formation of bis-glutathione (GS-SG), both these two effects contributing to cause oxidative stress. [76] In this sense, it can be envisaged that the Ag(I)-derived compound A may also trigger oxidative stress in *C. glabrata* cells thereby leading the cells to promote the up-regulation of the above-mentioned genes.

An interesting observation concerning protein and peptide degradation was the coordinate up-regulation of 7 genes encoding proteins belonging to the yapsin family including: *YPS2*, *YPS5*, *YPS6*, *YPS8*, *YPS9*, *YPS10* and *YPS11* (Table 3.2). The *YPS* gene family encodes extracellular glycosylphosphatidylinositol-linked aspartyl proteases, which are required for cell wall integrity, adherence to mammalian cells, survival in macrophages and virulence in *Candida glabrata*. [77] In 2007, Kaur *et al.* studied the relevance of the YPS cluster in *C. glabrata,* proving that the Yps proteases played an important role in remodeling the cell surface by removal of certain GPI-anchored cell wall proteins (GPI-CWPs) in response to different host environments. [77] This allows the subsequent incorporation of other cell wall proteins more suited to a given environment, suggesting that exposure to compound A may somehow perturb the cell wall structure, as shown for other chemicals in *C. glabrata.* [58, 62, 63], this being a hypothesis that requires further testing.

The down-regulated functions as a response to compound A with the highest relative frequency values in the dataset were DNA processing and RNA synthesis. However, since these functions are generally included in the general cellular response to environmental stress and are not substantially

informative *per se*, a closer analysis was done on the down-regulation of siderophore-iron transport and sugar transport.

With concern to siderophore-iron transport, a set of genes involved in metabolism and allocation of iron and copper in *C. glabrata* cells was identified, namely: SIT1, FET3, AFT1, FTR1 and CAGL0J07980g (Table 3.3). The repression of genes involved in iron and copper uptake in *C. glabrata* upon exposure to compound A might indicate that the cells sense the increase in metal concentration due to the silver present in the Ag(I)-camphorimine complexes and attempt to prevent its crossing through the membrane. Genes involved in iron ion homeostasis were found to be down-regulated upon *S. cerevisiae* exposure to various transition metals, silver included. [78] Additionally, it was also noticeable among the set of down-regulated genes several encoding hexose transporters including HXT1, HXT3, HXT4, HXT4/6/7 and HXT 6/7 (Table 3.3). Glucose sensing and transportation are highly regulated processes in most organisms, as glucose is an important source of carbon and energy. Therefore, when yeast cells are exposed to environmental stresses, such as antifungals, there is generally an up-regulation of glucose sensors and transporters as a means of ensuring that the cells will not starve and will have sufficient energy to overcome the stress they are being submitted to. [79, 80] However, in *S. cerevisiae*, two genes encoding glucose transporters – *HXT9* and *HXT11* – were found to be involved in the yeast's uptake of drugs, hence their deletion caused resistance to several drugs such as cycloheximide and sulfometuron methyl. [81] It could be hypothesized that the down-regulation of *HXT* genes verified in *C. glabrata* upon exposure to compound A might constitute an attempt of the yeast cells to avoid the uptake of this Ag(I)-camphorimine complex.

3.5. Efficacy of new Ag(I)-derived compounds against *C. glabrata*

Despite its high anti-*C. glabrata* potential, compound A was found to exhibit a high toxicity against mammalian cell lines (results not published) and therefore two other compounds (named B and C), obtained with a different chemical synthesis route without including nitrate in their composition were produced. The chemical formulas of compounds B and C are, respectively, $\{Ag(CCA\text{-}Li)_2(CCA)\}$ and $\{Ag_2(CCA)_2(CCA\text{-}Li)\}$ and their structures are shown in Figure 1.8. The efficiency of these two complexes was tested using a microdilution assay, in order to determine the corresponding MIC_{50} values against *C. glabrata* and *C. parapsilosis*. The assays were conducted at two pHs, 5 and 7, considering that efficacy of compound A was also found to change in a pH-dependent manner being more active at a neutral pH. [57] While compound B had little effect in inhibiting growth of the two *Candida* species tested, a very significant effect was observed for compound C resulting in MIC_{50} values of 62,5 mg/L for *C. glabrata* and 15,63 mg/L for *C. parapsilosis* (Figure 3.8 C and D). The lack of antimicrobial efficiency of ligand 1 alone (Figure 3.8 B) was not unexpected, given that in a similar work [56], in which Ag(I)-camphorimine compounds were also tested for their anti-*Candida* potential, the ligands of the majority of compounds were not effective in inhibiting fungal growth by themselves. As expected, no significant effect was observed for ethanol, used for solubilization of the two compounds (Figure 3.8 A). Also, as observed for compound A, activity was much more significant at pH 7 than at pH 5.

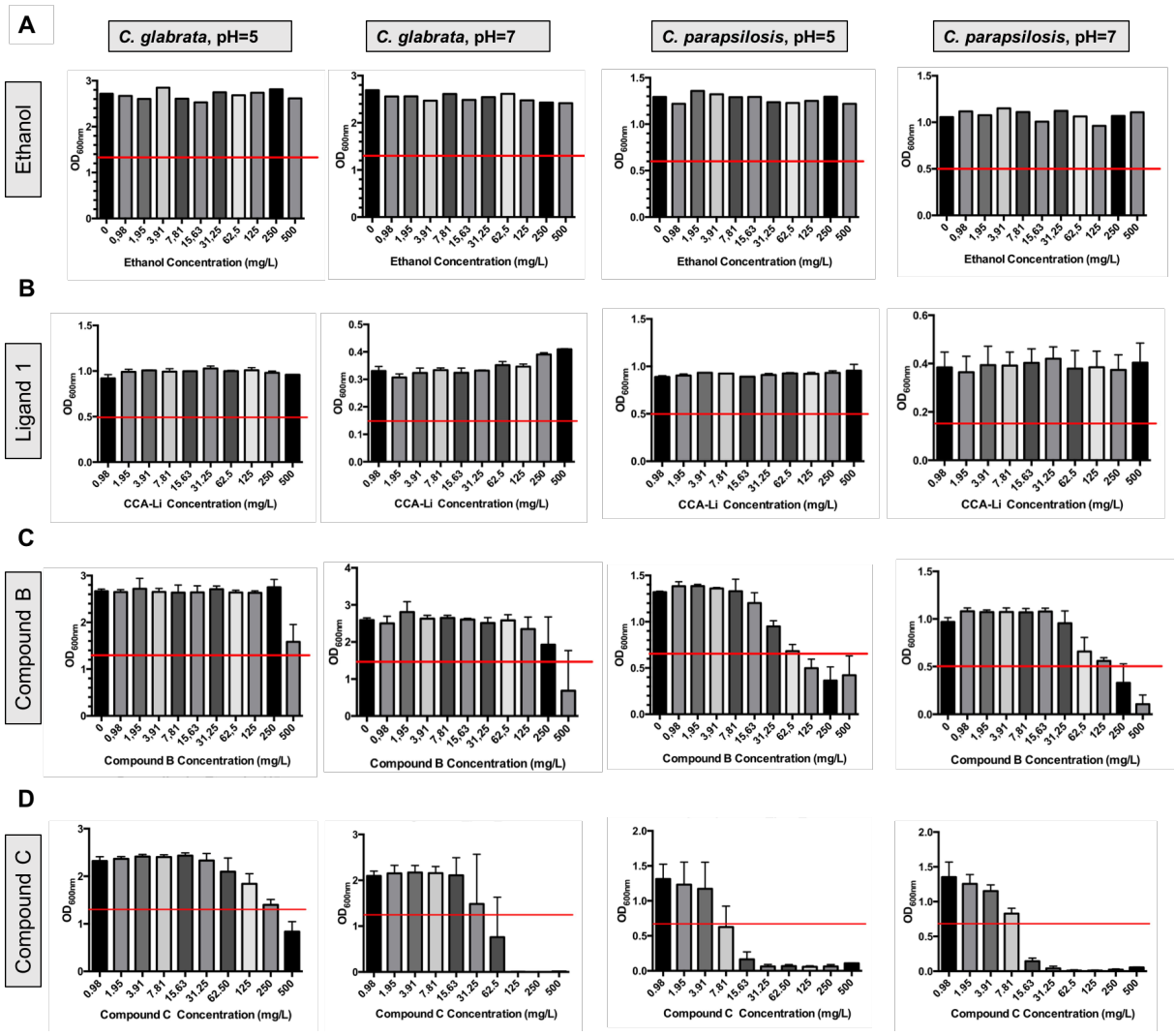

Figure 3.8 - A) Microdilution assays performed using *C. glabrata* and *C. parapsilosis* at pH 5 and 7 to determine if ethanol alone had an inhibitory effect; B) Microdilution assays performed using *C. glabrata* and *C. parapsilosis* at pH 5 and 7 to determine if the ligand CCA-Li alone had an inhibitory effect; C) Microdilution assays performed using *C. glabrata* and *C. parapsilosis* at pH 5 and 7 to determine the inhibitory effect of compound B; D) Microdilution assays performed using *C. glabrata* and *C. parapsilosis* at pH 5 and 7 to determine the inhibitory effect of compound C. The red lines mark the cell density correspondent to 50% of the full population.

The effect of pH on *in vitro* susceptibility of *Candida* spp. to drugs has been reported previously, more specifically in Danby *et al.* which were able to prove that for a wide variety of antifungals there was a noticeable increase in MIC_{50} values with the decrease in pH. [82]

Given that compounds B and C were able to inhibit growth of *C. glabrata*, albeit at different extents, their ability to inhibit growth of the set of azole-resistant isolates used in subchapter 3.1 of this thesis was examined. Once again, a microdilution assay was performed and the isolates FFUL412, FFUL443, FFUL674, FFUL830, FFUL866, and FFUL887, were grown in the presence of these compounds and in RPMI medium at pH 5 and 7. Additionally, since the compounds were dissolved in ethanol, cells were also grown in the presence of 70% EtOH as a negative control. The results obtained are depicted in Figures 3.9 and 3.10.

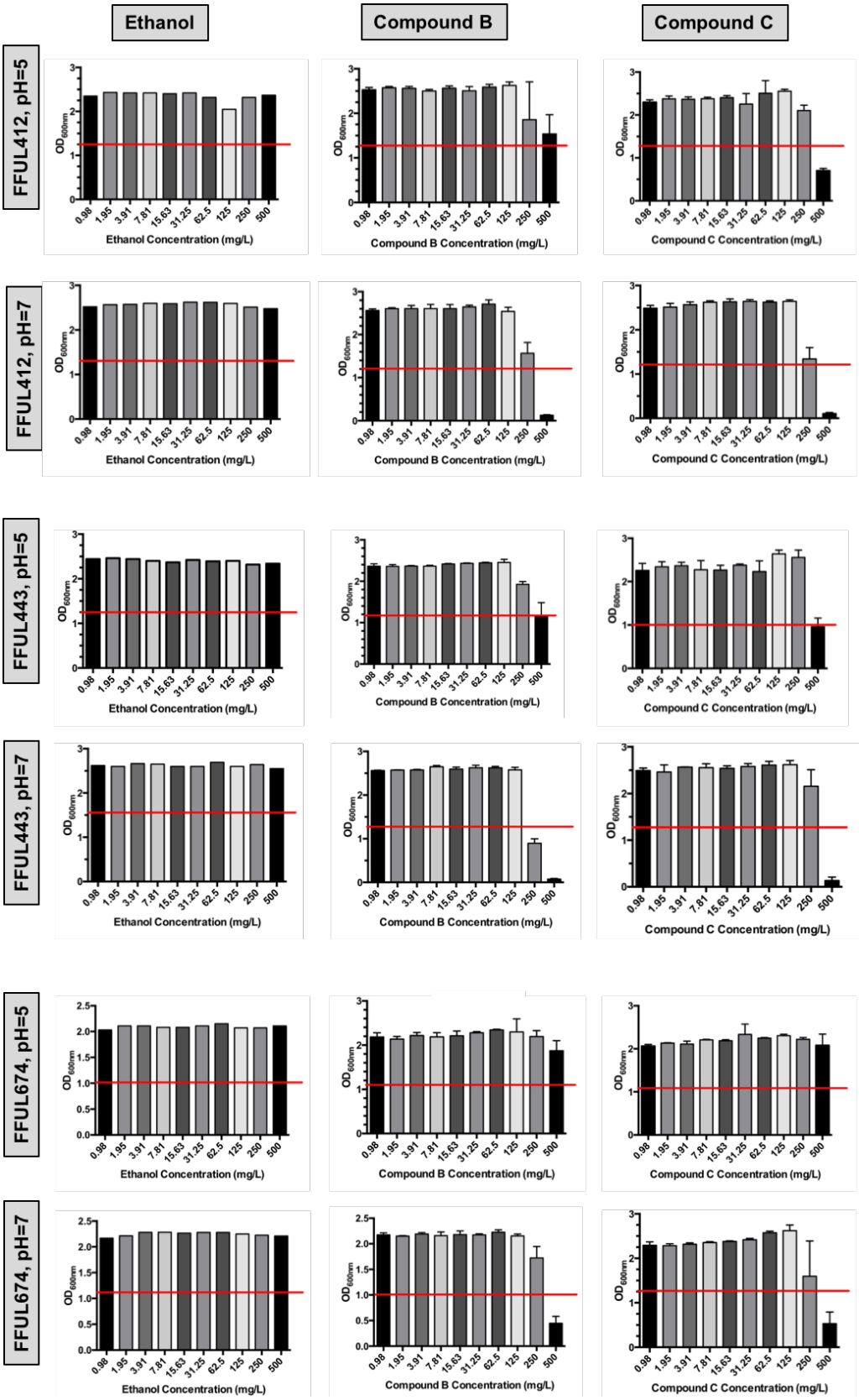

Figure 3.9 - Microdilution assays performed using three azole-resistant *C. glabrata* isolates – FFUL412, FFUL443 and FFUL674 – at pH 5 and 7 to determine the inhibitory effect of compounds B and C. Cells were also grown in the presence of ethanol to determine if this chemical alone had any inhibitory potential. The red lines mark the cell density correspondent to 50% of the full population.

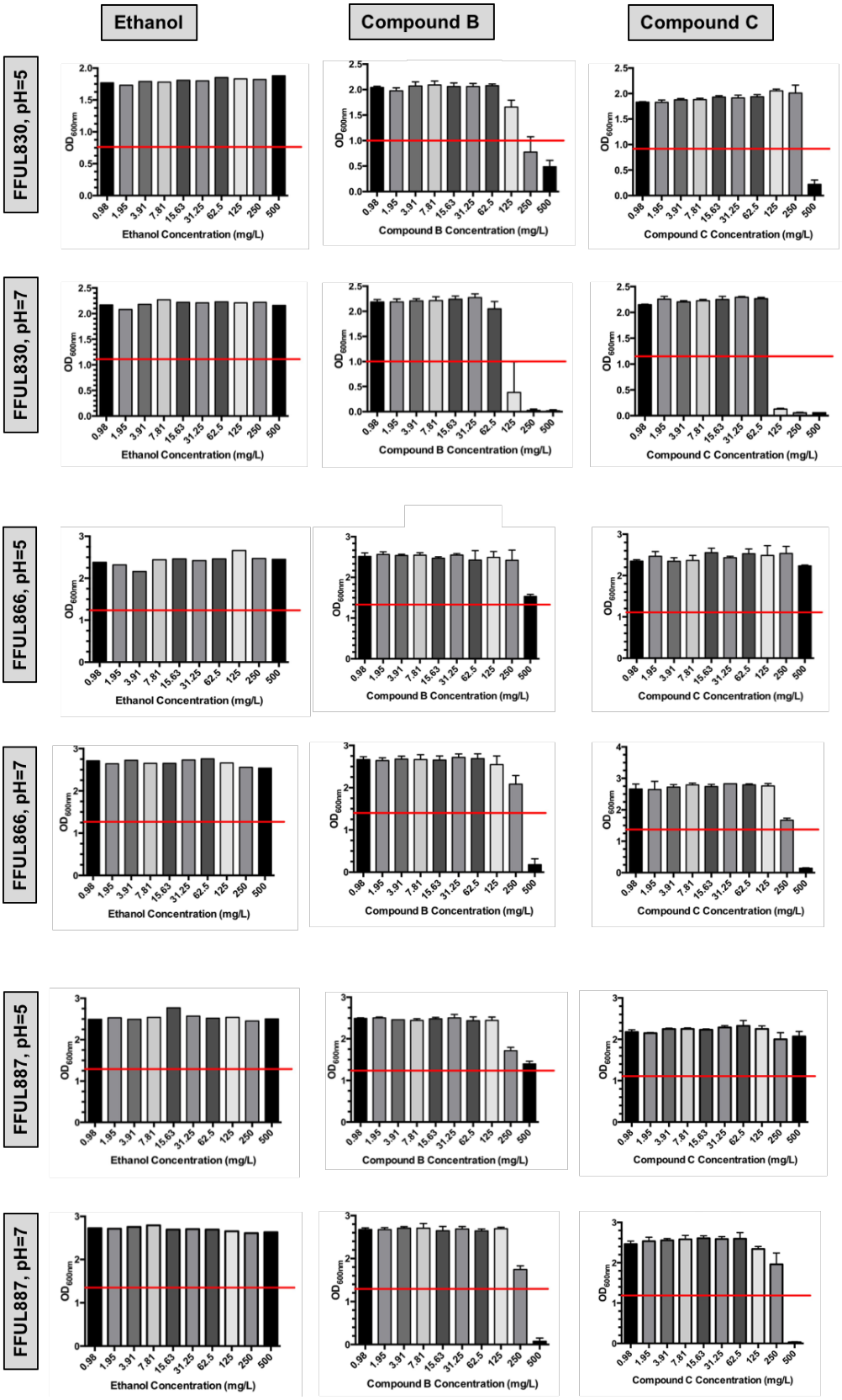

Figure 3.10 - Microdilution assays performed using three azole-resistant *C. glabrata* isolates – FFUL830, FFUL866 and FFUL887– at pH 5 and 7 to determine the inhibitory effect of compounds B and C. Cells were also grown in the presence of ethanol to determine if this chemical alone had any inhibitory potential. The red lines mark the cell density correspondent to 50% of the full population.

It was possible to confirm that any inhibitory effect observed was exclusively attributable to the presence of the Ag(I)-derived complexes since ethanol alone never had a significant deleterious effect over the growth of neither one of the tested isolates (Figures 3.9 and 3.10). Moreover, once more the pH-dependency [82] of the efficiency of compounds B and C was proven, since the results obtained revealed a higher efficacy in inhibiting cell growth at pH 7 than at pH 5 for both compounds (Figures 3.9 and 3.10).

The results obtained showed that compounds B and C were able to inhibit cellular growth of all the azole-resistant clinical isolates tested at minimal inhibitory concentrations ranging between 125 and 500 mg/L, with the lowest MIC_{50} values being observed for isolate FFUL830. Overall there were no significant differences identified in MIC_{50} values for each compound against the same isolate, however, for isolate FFUL443 (Figure 3.9) the MIC_{50} value for compound B was lower (250 mg/L) than for compound C (500 mg/L) indicating that the latter might be less efficient against this particular isolate. The fact that the Ag(I)-camphorimine complexes displayed a reduced inhibitory efficiency against the azole-resistant strains when compared to the wild-type CBS138 reference strain suggests that these drugs may inhibit *C. glabrata* growth through a mechanism not so different from the one triggered by the presence of azoles.

4. Concluding remarks

This thesis was aimed at tackling the increasing problem of acquired resistance to antifungals in the human pathogen *Candida glabrata.* This was done resorting to a multifaceted approach which combined the unveiling of the impact of *CgPDR1* gain-of-function mutations, the study of these mutations in the activity of the transcriptional regulator and the assessment of potential novel anti-*Candida* compounds.

Profiling of *CgCDR1* and *CgPUP1*, two genes that are used as hallmarks of CgPdr1 GOF mutants [47], in a cohort of 10 *C. glabrata* fluconazole- and voriconazole-resistant isolates suggested that the E5K, R35K, I392M and G558C amino acid substitutions could constitute new gain-of-function mutants of CgPdr1. To confirm that, the E5K, R35K and I392M amino acid substitutions together with a K274Q substitution (previously identified as a GOF mutation [50]) were recreated through site-directed mutagenesis using a pSP76 vector containing the *CgPDR1* gene, which was later used to transform four laboratory strains – *S. cerevisiae* BY4741, *S. cerevisiae* BY4741 ∆pdr1, *C. glabrata* ∆ura and *C. glabrata* SKY107 – in order to assess the effect of each substitution and of the wild-type *CgPDR1* allele in tolerance to fluconazole. Overall, the results obtained both in *S. cerevisiae* and in *C. glabrata* strongly confirmed the effect of the K274Q (this being in line with previous results from our lab [50]), the E5K and the I392M amino acid substitutions as new gain-of-function mutations in CgPdr1 since expression of *CgPDR1* alleles having only these substitutions improved growth of *C. glabrata* and *S. cerevisae* in the presence of fluconazole, in comparison with the protective effect exerted by the wild-type *CgPDR1* allele alone.

These newly-uncovered gain-of-function mutations add up to the increasingly long list of known CgPdr1 GOF variants conferring azole resistance to *C. glabrata*, further contributing to improve the diagnostic of patients and allowing the adjustment of current tools used in clinical therapies, however it remains unclear how these mutations affect the biochemical activity of CgPdr1. The point substitutions identified in CgPdr1 so far were observed to occur throughout the various domains of the protein [27, 31, 39] such as near the regulatory domain, as is the case for substitutions K274Q and I392M. Alterations such as these in the regulatory domain of CgPdr1 can result in gain-of-function mutations by counteracting the negative action of this domain or by altering the binding of the drugs to the protein, eventually bypassing the need of drug-binding to promote activation. However, up to this point and to the best of our knowledge, no GOF mutations associated with azole-resistance in *C. glabrata* have been identified near the DNA binding domain, as is the case for the E5K amino acid substitution. The DNA-binding domain of CgPdr1 is responsible for binding of the regulator to the DNA motif PDRE found in the promoter region of its target genes [42], therefore the E5K replacement could promote constitutive activation of this regulator, however further studies are required to better understand how this replacement may affect binding of CgPdr1 to its target sequence and the interaction with the transcriptional machinery.

Although there are several GOF mutations already described in CgPdr1, little is known of how these mutations affect the overall biochemical activity of the protein and this work also intended to provide some advances in that field. Thus, it was investigated how the K274Q replacement would affect the CgPdr1 activity and a strategy to assess how this SNP could contribute for the

transactivation potential of the regulator was designed. Unfortunately, the underlying cloning procedures were not successful during the time of this thesis, however, this remains a key topic deserving further investigation.

In a second line of work, to better understand how Ag(I)-camphorimine complexes inhibit growth of *Candida glabrata*, a transcriptomics approach based on species-specific DNA microarrays was used. More specifically, it was assessed how *C. glabrata* cells respond to a toxic, but not lethal, concentration of the Ag(I)-derived compound A. Results from the transcriptomic analysis suggested that compound A triggers oxidative stress in *C. glabrata,* leads to methionine depletion and may somehow interfere with the cell wall structure and the uptake of iron in these cells. Future studies are required to confirm this hypothesis raised by the genomic expression analysis, such as, for example, conducting an assay with isotope-labeled methionine and evaluating the variations in concentration of this amino acid when *C. glabrata* cells are grown in the presence or absence of compound A. Compounds B and C were also herein shown to exert an important inhibitory effect against *C. glabrata*, albeit their inhibitory efficiency being lower than the one observed for compound A. These results reinforce the relevance of Ag(I)-camphorimine complexes as promising novel antifungal agents. Despite these positive insights, there are still issues to overcome before these compounds can be introduced into clinical practice. In fact, despite the recognized antimicrobial activity of silver salts such as silver nitrate, the pharmacological application of silver derivatives has been restricted mostly to external uses due to toxicity concerns. Recent studies showed that silver nitrate and silver nanoparticles have no significant toxicity in a murine model [83] however further toxicity analysis must be conducted with Ag(I)-camphorimine complexes to ensure that their use as antifungals continues to display more advantages than disadvantages.

5. References

1. Whibley, N. and S.L. Gaffen, *Beyond Candida albicans: Mechanisms of immunity to non-albicans Candida species.* Cytokine, 2015. **76**(1): p. 42-52.
2. Papon, N., et al., *Emerging and emerged pathogenic Candida species: beyond the Candida albicans paradigm.* PLoS Pathog, 2013. **9**(9): p. e1003550.
3. d'Enfert, C., *Hidden killers: persistence of opportunistic fungal pathogens in the human host.* Curr Opin Microbiol, 2009. **12**(4): p. 358-64.
4. Sardi, J.C., et al., *Candida species: current epidemiology, pathogenicity, biofilm formation, natural antifungal products and new therapeutic options.* J Med Microbiol, 2013. **62**(Pt 1): p. 10-24.
5. Rautemaa-Richardson, R. and M.D. Richardson, *Systemic Fungal Infections.* Medicine, 2017. **45**(12): p. 757-762.
6. Boualem Sendid, J.L.P., Marc Tabouret, Alain Bonnin, Denis Caillot, Daniel Camus and Daniel Poulain, *Combined detection of mannanaemia and anti-mannan antibodies as a strategy for the diagnosis of systemic infection caused by pathogenic Candida species.* Journal of Medical Microbiology, 2001. **51**(2002): p. 433-442.
7. Hirano, R., et al., *Retrospective analysis of mortality and Candida isolates of 75 patients with candidemia: a single hospital experience.* Infect Drug Resist, 2015. **8**: p. 199-205.
8. Healey, K.R., et al., *Genetic Drivers of Multidrug Resistance in Candida glabrata.* Front Microbiol, 2016. **7**: p. 1995.
9. Graybill, J.R. and P.C. Craven, *Antifungal agents used in systemic mycoses. Activity and therapeutic use.* Drugs, 1983. **25**(1): p. 41-62.
10. Nguyen, M.H., et al., *The changing face of candidemia: emergence of non-Candida albicans species and antifungal resistance.* Am J Med, 1996. **100**(6): p. 617-23.
11. Morace, G., F. Perdoni, and E. Borghi, *Antifungal drug resistance in Candida species.* J Glob Antimicrob Resist, 2014. **2**(4): p. 254-259.
12. Whaley, S.G. and P.D. Rogers, *Azole Resistance in Candida glabrata.* Curr Infect Dis Rep, 2016. **18**(12): p. 41.
13. Nucci, M. and K.A. Marr, *Emerging fungal diseases.* Clin Infect Dis, 2005. **41**(4): p. 521-6.
14. Deorukhkar, S.C., S. Saini, and S. Mathew, *Non-albicans Candida Infection: An Emerging Threat.* Interdiscip Perspect Infect Dis, 2014. **2014**: p. 615958.
15. Falagas, M.E., N. Roussos, and K.Z. Vardakas, *Relative frequency of albicans and the various non-albicans Candida spp among candidemia isolates from inpatients in various parts of the world: a systematic review.* Int J Infect Dis, 2010. **14**(11): p. e954-66.
16. Neppelenbroek, K.H., et al., *Identification of Candida species in the clinical laboratory: a review of conventional, commercial, and molecular techniques.* Oral Dis, 2014. **20**(4): p. 329-44.
17. Sabino, R., et al., *Serious fungal infections in Portugal.* Eur J Clin Microbiol Infect Dis, 2017. **36**(7): p. 1345-1352.
18. Faria-Ramos, I., et al., *Species distribution and in vitro antifungal susceptibility profiles of yeast isolates from invasive infections during a Portuguese multicenter survey.* Eur J Clin Microbiol Infect Dis, 2014. **33**(12): p. 2241-7.

19. Correia, A., et al., *Study of molecular epidemiology of candidiasis in portugal by PCR fingerprinting of Candida clinical isolates.* J Clin Microbiol, 2004. **42**(12): p. 5899-903.
20. Paulo, C., et al., *Retrospective analysis of clinical yeast isolates in a hospital in the centre of Portugal: spectrum and revision of the identification procedures.* Med Mycol, 2009. **47**(8): p. 836-44.
21. Mast, N., et al., *Antifungal Azoles: Structural Insights into Undesired Tight Binding to Cholesterol-Metabolizing CYP46A1.* Mol Pharmacol, 2013. **84**(1): p. 86-94.
22. Maubon, D., et al., *Resistance of Candida spp. to antifungal drugs in the ICU: where are we now?* Intensive Care Med, 2014. **40**(9): p. 1241-55.
23. Kathiravan, M.K., et al., *The biology and chemistry of antifungal agents: a review.* Bioorg Med Chem, 2012. **20**(19): p. 5678-98.
24. Kelly, S.L., et al., *Mode of action and resistance to azole antifungals associated with the formation of 14 alpha-methylergosta-8,24(28)-dien-3 beta,6 alpha-diol.* Biochem Biophys Res Commun, 1995. **207**(3): p. 910-5.
25. Sanguinetti, M., et al., *Mechanisms of azole resistance in clinical isolates of Candida glabrata collected during a hospital survey of antifungal resistance.* Antimicrob Agents Chemother, 2005. **49**(2): p. 668-79.
26. Hull, C.M., et al., *Facultative sterol uptake in an ergosterol-deficient clinical isolate of Candida glabrata harboring a missense mutation in ERG11 and exhibiting cross-resistance to azoles and amphotericin B.* Antimicrob Agents Chemother, 2012. **56**(8): p. 4223-32.
27. Tsai, H.F., et al., *Microarray and molecular analyses of the azole resistance mechanism in Candida glabrata oropharyngeal isolates.* Antimicrob Agents Chemother, 2010. **54**(8): p. 3308-17.
28. Sanglard, D. and F.C. Odds, *Resistance of Candida species to antifungal agents: molecular mechanisms and clinical consequences.* Lancet Infect Dis, 2002. **2**(2): p. 73-85.
29. Whaley, S.G., et al., *Azole Antifungal Resistance in Candida albicans and Emerging Non-albicans Candida Species.* Front Microbiol, 2016. **7**: p. 2173.
30. Costa, C., et al., *MFS multidrug transporters in pathogenic fungi: do they have real clinical impact?* Front Physiol, 2014. **5**: p. 197.
31. Caudle, K.E., et al., *Genomewide expression profile analysis of the Candida glabrata Pdr1 regulon.* Eukaryot Cell, 2011. **10**(3): p. 373-83.
32. Costa, C., et al., *Clotrimazole Drug Resistance in Candida glabrata Clinical Isolates Correlates with Increased Expression of the Drug:H(+) Antiporters CgAqr1, CgTpo1_1, CgTpo3, and CgQdr2.* Front Microbiol, 2016. **7**: p. 526.
33. Tsai, H.F., et al., *Candida glabrata PDR1, a transcriptional regulator of a pleiotropic drug resistance network, mediates azole resistance in clinical isolates and petite mutants.* Antimicrob Agents Chemother, 2006. **50**(4): p. 1384-92.
34. Singh-Babak, S.D., et al., *Global analysis of the evolution and mechanism of echinocandin resistance in Candida glabrata.* PLoS Pathog, 2012. **8**(5): p. e1002718.
35. Brun, S., et al., *Mechanisms of azole resistance in petite mutants of Candida glabrata.* Antimicrob Agents Chemother, 2004. **48**(5): p. 1788-96.

36. Sanglard, D., F. Ischer, and J. Bille, *Role of ATP-binding-cassette transporter genes in high-frequency acquisition of resistance to azole antifungals in Candida glabrata.* Antimicrob Agents Chemother, 2001. **45**(4): p. 1174-83.
37. Vermitsky, J.P. and T.D. Edlind, *Azole resistance in Candida glabrata: coordinate upregulation of multidrug transporters and evidence for a Pdr1-like transcription factor.* Antimicrob Agents Chemother, 2004. **48**(10): p. 3773-81.
38. Sanglard, D., et al., *The ATP binding cassette transporter gene CgCDR1 from Candida glabrata is involved in the resistance of clinical isolates to azole antifungal agents.* Antimicrob Agents Chemother, 1999. **43**(11): p. 2753-65.
39. Ferrari, S., et al., *Gain of function mutations in CgPDR1 of Candida glabrata not only mediate antifungal resistance but also enhance virulence.* PLoS Pathog, 2009. **5**(1): p. e1000268.
40. Vermitsky, J.P., et al., *Pdr1 regulates multidrug resistance in Candida glabrata: gene disruption and genome-wide expression studies.* Mol Microbiol, 2006. **61**(3): p. 704-22.
41. Rogers, B., et al., *The pleitropic drug ABC transporters from Saccharomyces cerevisiae.* J Mol Microbiol Biotechnol, 2001. **3**(2): p. 207-14.
42. MacPherson, S., M. Larochelle, and B. Turcotte, *A fungal family of transcriptional regulators: the zinc cluster proteins.* Microbiol Mol Biol Rev, 2006. **70**(3): p. 583-604.
43. Todd, R.B. and A. Andrianopoulos, *Evolution of a fungal regulatory gene family: the Zn(II)2Cys6 binuclear cluster DNA binding motif.* Fungal Genet Biol, 1997. **21**(3): p. 388-405.
44. Thakur, J.K., et al., *A nuclear receptor-like pathway regulating multidrug resistance in fungi.* Nature, 2008. **452**(7187): p. 604-9.
45. Goffeau, A., *Drug resistance: the fight against fungi.* Nature, 2008. **452**(7187): p. 541-2.
46. Nishikawa, J.L., et al., *Inhibiting fungal multidrug resistance by disrupting an activator-Mediator interaction.* Nature, 2016. **530**(7591): p. 485-9.
47. Ferrari, S., et al., *Contribution of CgPDR1-regulated genes in enhanced virulence of azole-resistant Candida glabrata.* PLoS One, 2011. **6**(3): p. e17589.
48. Torelli, R., et al., *The ATP-binding cassette transporter-encoding gene CgSNQ2 is contributing to the CgPDR1-dependent azole resistance of Candida glabrata.* Mol Microbiol, 2008. **68**(1): p. 186-201.
49. Berila, N., et al., *Mutations in the CgPDR1 and CgERG11 genes in azole-resistant Candida glabrata clinical isolates from Slovakia.* Int J Antimicrob Agents, 2009. **33**(6): p. 574-8.
50. S. B. Salazar, C.W., M. Münsterkötter, M. Okamoto, A. Takahashi-Nakaguchi, H. Chibana, M. M. Lopes, U. Güldener, G. Butler, N. P. Mira, *Comparative genomic and transcriptomic analyses unveil novel features of azole resistance and adaptation to the human host in Candida glabrata.* FEMS Yeast Research, 2017. **18**(1): p. 1-11.
51. Paul, S., J.A. Schmidt, and W.S. Moye-Rowley, *Regulation of the CgPdr1 transcription factor from the pathogen Candida glabrata.* Eukaryot Cell, 2011. **10**(2): p. 187-97.
52. Khakhina, S., L. Simonicova, and W.S. Moye-Rowley, *Positive autoregulation and repression of transactivation are key regulatory features of the Candida glabrata Pdr1 transcription factor.* Mol Microbiol, 2018. **107**(6): p. 747-764.

53. Vandeputte, P., S. Ferrari, and A.T. Coste, *Antifungal resistance and new strategies to control fungal infections.* Int J Microbiol, 2012. **2012**: p. 713687.
54. Pianalto, K.M. and J.A. Alspaugh, *New Horizons in Antifungal Therapy.* J Fungi (Basel), 2016. **2**(4).
55. Rai, M., A. Yadav, and A. Gade, *Silver nanoparticles as a new generation of antimicrobials.* Biotechnol Adv, 2009. **27**(1): p. 76-83.
56. Cardoso, J.M.S., et al., *Ag(I) camphorimine complexes with antimicrobial activity towards clinically important bacteria and species of the Candida genus.* PLoS One, 2017. **12**(5): p. e0177355.
57. Novais, D.S., *Studying mechanisms of antifungal resistance in Candida glabrata clinical isolates: emphasis on the role of the CgPdr1 transcription factor*, in *Departamento de Biologia Vegetal*. 2018, Universidade de Lisboa: Faculdade de Ciências
58. Panacek, A., et al., *Silver colloid nanoparticles: synthesis, characterization, and their antibacterial activity.* J Phys Chem B, 2006. **110**(33): p. 16248-53.
59. Panacek, A., et al., *Antifungal activity of silver nanoparticles against Candida spp.* Biomaterials, 2009. **30**(31): p. 6333-40.
60. Kim, K.J., et al., *Antifungal activity and mode of action of silver nano-particles on Candida albicans.* Biometals, 2009. **22**(2): p. 235-42.
61. Monteiro, D.R., et al., *Silver colloidal nanoparticles: antifungal effect against adhered cells and biofilms of Candida albicans and Candida glabrata.* Biofouling, 2011. **27**(7): p. 711-9.
62. Munoz, J.E., et al., *Antifungal Activity of the Biphosphinic Cyclopalladate C7a against Candida albicans Yeast Forms In Vitro and In Vivo.* Front Microbiol, 2017. **8**: p. 771.
63. Li, H., et al., *In vitro and in vivo antifungal activities and mechanism of heteropolytungstates against Candida species.* Sci Rep, 2017. **7**(1): p. 16942.
64. Reddy, K.V., R.D. Yedery, and C. Aranha, *Antimicrobial peptides: premises and promises.* Int J Antimicrob Agents, 2004. **24**(6): p. 536-47.
65. Tam, J.P., et al., *Antimicrobial Peptides from Plants.* Pharmaceuticals (Basel), 2015. **8**(4): p. 711-57.
66. Katiyar, S., M. Pfaller, and T. Edlind, *Candida albicans and Candida glabrata clinical isolates exhibiting reduced echinocandin susceptibility.* Antimicrob Agents Chemother, 2006. **50**(8): p. 2892-4.
67. Keller, G., et al., *Haa1, a protein homologous to the copper-regulated transcription factor Ace1, is a novel transcriptional activator.* J Biol Chem, 2001. **276**(42): p. 38697-702.
68. Katiyar, S., et al., *Evaluation of Polymorphic Locus Sequence Typing for Candida glabrata Epidemiology.* J Clin Microbiol, 2016. **54**(4): p. 1042-50.
69. Hill, J.A., T.R. O'Meara, and L.E. Cowen, *Fitness Trade-Offs Associated with the Evolution of Resistance to Antifungal Drug Combinations.* Cell Rep, 2015.
70. Pavelka, N., et al., *Aneuploidy confers quantitative proteome changes and phenotypic variation in budding yeast.* Nature, 2010. **468**(7321): p. 321-5.

71. Popp, C., et al., *Competitive Fitness of Fluconazole-Resistant Clinical Candida albicans Strains.* Antimicrob Agents Chemother, 2017. **61**(7).
72. Ruepp, A., et al., *The FunCat, a functional annotation scheme for systematic classification of proteins from whole genomes.* Nucleic Acids Res, 2004. **32**(18): p. 5539-45.
73. Monteiro, P.T., et al., *The PathoYeastract database: an information system for the analysis of gene and genomic transcription regulation in pathogenic yeasts.* Nucleic Acids Res, 2017. **45**(D1): p. D597-D603.
74. Vicky W.-M.Lee, H.L., Tai-Chu Lau, Roger Guevremont and K.W. Michael Siu, *Relative silver(I) ion binding energies of α-amino acids: a determination by means of the kinetic method.* Journal of the American Society for Mass Spectrometry, 1998. **9**(8): p. 760-766.
75. Wright, J.B., et al., *Efficacy of topical silver against fungal burn wound pathogens.* Am J Infect Control, 1999. **27**(4): p. 344-50.
76. Cuellar-Cruz, M., et al., *Biosynthesis of micro- and nanocrystals of Pb (II), Hg (II) and Cd (II) sulfides in four Candida species: a comparative study of in vivo and in vitro approaches.* Microb Biotechnol, 2017. **10**(2): p. 405-424.
77. Rupinder Kaur, B.M., and Brendan P. Cormack, *A family of glycosylphosphatidylinositol-linked aspartyl proteases is required for virulence of Candida glabrata.* Proceedings of the National Academy of Sciences of the United States of America, 2007. **104**(18): p. 7628–7633.
78. Jin, Y.H., et al., *Global transcriptome and deletome profiles of yeast exposed to transition metals.* PLoS Genet, 2008. **4**(4): p. e1000053.
79. Ng, T.S., et al., *Phylogenetic and Transcripts Profiling of Glucose Sensing Related Genes in Candida glabrata.* Jundishapur J Microbiol, 2015. **8**(11): p. e25177.
80. Pais, P., et al., *Membrane Proteome-Wide Response to the Antifungal Drug Clotrimazole in Candida glabrata: Role of the Transcription Factor CgPdr1 and the Drug:H+ Antiporters CgTpo1_1 and CgTpo1_2.* Mol Cell Proteomics, 2016. **15**(1): p. 57-72.
81. Ozcan, S. and M. Johnston, *Function and regulation of yeast hexose transporters.* Microbiol Mol Biol Rev, 1999. **63**(3): p. 554-69.
82. Danby, C.S., et al., *Effect of pH on in vitro susceptibility of Candida glabrata and Candida albicans to 11 antifungal agents and implications for clinical use.* Antimicrob Agents Chemother, 2012. **56**(3): p. 1403-6.
83. Qin, G., et al., *Toxicological evaluation of silver nanoparticles and silver nitrate in rats following 28 days of repeated oral exposure.* Environ Toxicol, 2017. **32**(2): p. 609-618.

6. Annexes

Annex A

Table 6.1 - List of clinical isolates used in this thesis, the samples from which they were collected, and fluconazole and/or voriconazole minimal inhibitory concentration (in mg/L). ND – No data available.

Clinical Isolate	Sample	Fluconazole MIC (mg/L)	Voriconazole MIC (mg/L)
29	ND	64	8
56	ND	> 64	> 8
412	Bronchoalveolar	> 64	2
443	Bronchoalveolar	> 64	2
556	ND	> 64	> 4
607	ND	> 64	> 4
674	Bronchoalveolar	> 32	2
830	Urine	64	8
866	Urine	64	2
887	Urine	64	2

Annex B

```
CBS138_PDR1      MQTLETTSKSNPGEVKAQKPSTRRTKVGKACDSCRRRKIKCNGLKPCPSCTIYGCECTYT   60
IS29_PDR1        MQTLETTSKSNPGEVKAQKPSTRRTKVGKACDSCRRRKIKCNGLKPCPSCTIYGCECTYT   60
                 ************************************************************

CBS138_PDR1      DAKSTKNLKSNDAGKSKPTGRVSKNKETTRVDKDIRRLEQQYVPINANIHVGPRFPSENI   120
IS29_PDR1        DAKSTKNLKSNDAGKSKPTGRVSKNKETTRIDKDIRRSEQQYVPINANIHVGPRFPSENI   120
                 ********************************:***** ********************

CBS138_PDR1      LNGYPQCGAPQNNVVGNPLAVNTQCHRGLSETPMSSTFKESNLRDDRLLQSSDTDDMRNG   180
IS29_PDR1        LNGYPQCGAPQNNVVGNPLAVNTQCHRGLSETPMSSTFKESNLRDDRLLQSSDTDDMRNG   180
                 ************************************************************

CBS138_PDR1      DSEERDLKGSDSENVKSKDNKSDPLIIYKDDTHIESTVNKLTQAVNELKSLQNAPSSIKS   240
IS29_PDR1        DSEERDLKGSDSENVKSKDNKSDPLIIYKDDTHIESTVNKLTQAVNELKSLQNAPSSIKS   240
                 ************************************************************

CBS138_PDR1      SIQAIELQLRNILDNWKPEVDFEKAKINESATTKSLETNLLRNKYTNHVHLTRFRIWIDY   300
IS29_PDR1        SINAIELQLRNILDNWKPEVDFEKAKINESATTKSLETNLLRNKYTNHVHLTRFRIWIDY   300
                 **.*********************************************************

CBS138_PDR1      KNANKNNHFMGECGFSLAESFFASNQPLVDELFGLYSQVEAFSLQGLGYCVHLYEPYMKT   360
IS29_PDR1        KNANKNNHFMGECGFSLAESFFASNQPLVDELFGLYSQVEAFSLQGLGYCVHLYEPYMKT   360
                 ************************************************************

CBS138_PDR1      EEAIKLMKETLYIILRFIDICVHHINEESISIANPLETYLRKKHLMPMTPTPRSSYGSPQ   420
IS29_PDR1        EEAIKLMKETLYIILRFIDICVHHINEESISIANPLETYLRKKHLMPMTPTPRSSYGSPQ   420
                 ************************************************************

CBS138_PDR1      SASTKSLVSKIIERIPQPFIESVTNVSSLQLLDLRDDESKMFGTLLNMCKSIRRKFDSVM   480
IS29_PDR1        SASTKSLVSKIIERIPQPFIESVTNVSSLQLLDLRDDESKMFGTLLNMCKSIRRKFDSVM   480
                 ************************************************************

CBS138_PDR1      SDYDSIVTEKSEGEQNDGKVTVAEFTSLCEAEEMLLALCYNYYNLTLYSFFEFGTNIEYM   540
IS29_PDR1        SDYDSIVTEKSEGEQNDGKVTVAEFTSLCEAEEMLLALCYNYYNLTLYSFFEFGTNIEYM   540
                 ************************************************************

CBS138_PDR1      EHLLLLLEEQLALDEYYGFEKVLNVAVANAKKMGFHRWEFYVGYEESTAEKRRLLWWKLY   600
IS29_PDR1        EHLLLLLEEQLALDEYYGFEKVLNVAVANAKKMGFHRWEFYVGYEESTAEKRRLLWWKLY   600
                 ************************************************************

CBS138_PDR1      NYEKASTMKKGFFSVIDDATVNCLLPKIFRNFGYLDRVEFLENIQKPMDLSVFSDVPISV   660
IS29_PDR1        NYEKASTMKKGFFSVIDDATVNCLLPKIFRNFGYLDRVEFLENIQKPMDLSVFSDVPISV   660
                 ************************************************************

CBS138_PDR1      LCKYGELALTIVTSEFHEKFLYADRYTSIRNSAKPPTLKNQLIKEIVDGIAYTETSYEAI   720
IS29_PDR1        LCKYGELALTIVTSEFHEKFLYADRYTSIRNSAKPPTLKNQLIKEIVDGIAYTETSYEAI   720
                 ************************************************************

CBS138_PDR1      RKQTAKLWDIALGKVTKDKINKEDTAAASKFTLSYEYHRFRLINMADNLIARLMVKPKSD   780
IS29_PDR1        RKQTAKLWDIALGKVTKDKINKEDTAAASKFTLSYEYHRFRLINMADNLIARLMVKPKSD   780
                 ************************************************************

CBS138_PDR1      WLISVMKGHLNRLYEHWKVMNEIILSMDNDYSIATTFEYYAPSCLCLATQTFLIVRNMEM   840
IS29_PDR1        WLISVMKGHLNRLYEHWKVMNEIILSMDNDYSIATTFEYYAPSCLCLATQTFLIVRNMEM   840
                 ************************************************************

CBS138_PDR1      DDVKMMVAVYKRFLNLGMFLQSAKVCSLADSHTFRDFSRSFSFITIISRLMIIEFMQIKE   900
IS29_PDR1        DDVKMMVAVYKRFLNLGMFLQSAKVCSLADSHTFRDFSRSFSFITIISRLMIIEFMQIKE   900
                 ************************************************************

CBS138_PDR1      LTKVEFIEKFSEVCPDLADLPPMLLDPNSCLYFSLLQQIKKSGFTLSFKKILEDARMMDF   960
IS29_PDR1        LTKVEFIEKFSEVCPDLADLPPMLLDPNSCLYFSLLQQIKKSGFTLSFKKILEDARMMDF   960
                 ************************************************************

CBS138_PDR1      NYDRNLDSEAIKKCNGEFSKSMPSCTNVSDTTTAVSDNSAKKKASMGSARVNSTDTLTAS   1020
IS29_PDR1        NYDRNLDSEAIKKCNGEFSKSMPSCTNVSDTTTAVSDNSAKKKASMGSARVNSTDTLTAS   1020
                 ************************************************************

CBS138_PDR1      PLSGLRNQTQLDSKDSVPSLEAYTPIDSVSDVPTGEINVPFPPVYNQNGLDQQTTYNLGT   1080
IS29_PDR1        PLSGLRNQTQLDSKDSVPSLEAYTPIDSVSDVPTGEINVPFPPVYNQNGLDQQTTYNLGT   1080
                 ************************************************************

CBS138_PDR1      LDEFVNKGDLNELYNSLWGDLFSDVYL    1107
IS29_PDR1        LDEFVNKGDLNELYNSLWGDLFSDVYL    1107
                 ***************************
```

Figure 6.1 - Alignment of the *CgPDR1* sequence obtained from isolate FFUL29 with the sequence of the CBS138 reference strain. The sequencing reaction was performed by STABVIDA as a paid service and Clustal Omega was used for sequence alignment. Amino acid substitutions are represented by a red rectangle.

Annex C

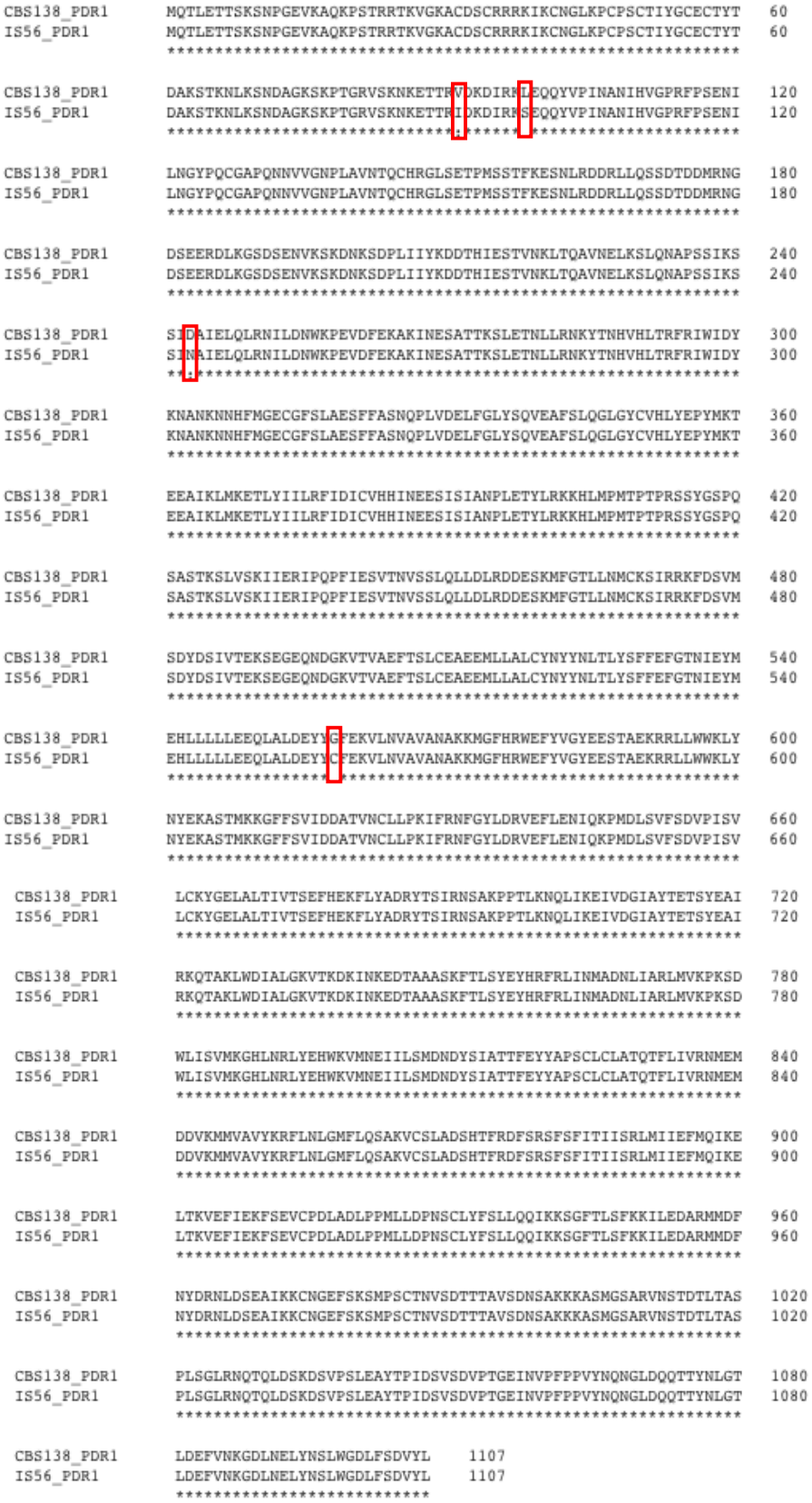

Figure 6.2 - Alignment of the *CgPDR1* sequence obtained from isolate FFUL56 with the sequence of the CBS138 reference strain. The sequencing reaction was performed by STABVIDA as a paid service and Clustal Omega was used for sequence alignment. Amino acid substitutions are represented by a red rectangle.

Annex D

```
CBS138_PDR1      MQTLETTSKSNPGEVKAQKPSTRRTKVGKACDSCRRRKIKCNGLKPCPSCTIYGCECTYT   60
IS556_PDR1       MQTLETTSKSNPGEVKAQKPSTRRTKVGKACDSCRRRKIKCNGLKPCPSCTIYGCECTYT   60
                 ************************************************************

CBS138_PDR1      DAKSTKNLKSNDAGKSKPTGRVSKNKETTRVDKDIRNLEQQYVPINANIHVGPRFPSENI   120
IS556_PDR1       DAKSTKNLKSNDAGKSKPTGRVSKNKETTRIDKDIRNSEQQYVPINANIHVGPRFPSENI   120
                 ********************************.*****.*********************

CBS138_PDR1      LNGYPQCGAPQNNVVGNPLAVNTQCHRGLSETPMSSTFKESNLRDDRLLQSSDTDDMRNG   180
IS556_PDR1       LNGYPQCGAPQNNVVGNPLAVNTQCHRGLSETPMSSTFKESNLRDDRLLQSSDTDDMRNG   180
                 ************************************************************

CBS138_PDR1      DSEERDLKGSDSENVKSKDNKSDPLIIYKDDTHIESTVNKLTQAVNELKSLQNAPSSIKS   240
IS556_PDR1       DSEERDLKGSDSENVKSKDNKSDPLIIYKDDTHIESTVNKLTQAVNELKSLQNAPSSIKS   240
                 ************************************************************

CBS138_PDR1      SIDAIELQLRNILDNWKPEVDFEKAKINESATTKSLETNLLRNKYTNHVHLTRFRIWIDY   300
IS556_PDR1       SINAIELQLRNILDNWKPEVDFEKAKINESATTKSLETNLLRNKYTNHVHLTRFRIWIDY   300
                 **.************************************************************

CBS138_PDR1      KNANKNNHFMGECGFSLAESFFASNQPLVDELFGLYSQVEAFSLQGLGYCVHLYEPYMKT   360
IS556_PDR1       KNANKNNHFMGECGFSLAESFFASNQPLVDELFGLYSQVEAFSLQGLGYCVHLYEPYMKT   360
                 ************************************************************

CBS138_PDR1      EEAIKLMKETLYIIIRFIDICVHHINEESISIANPLETYLRKKHLMPMTPTPRSSYGSPQ   420
IS556_PDR1       EEAIKLMKETLYIIIWFIDICVHHINEESISIANPLETYLRKKHLMPMTPTPRSSYGSPQ   420
                 **********.*************************************************

CBS138_PDR1      SASTKSLVSKIIERIPQPFIESVTNVSSLQLLDLRDDESKMFGTLLNMCKSIRRKFDSVM   480
IS556_PDR1       SASTKSLVSKIIERIPQPFIESVTNVSSLQLLDLRDDESKMFGTLLNMCKSIRRKFDSVM   480
                 ************************************************************

CBS138_PDR1      SDYDSIVTEKSEGEQNDGKVTVAEFTSLCEAEEMLLALCYNYYNLTLYSFFEFGTNIEYM   540
IS556_PDR1       SDYDSIVTEKSEGEQNDGKVTVAEFTSLCEAEEMLLALCYNYYNLTLYSFFEFGTNIEYM   540
                 ************************************************************

CBS138_PDR1      EHLLLLLEEQLALDEYYGFEKVLNVAVANAKKMGFHRWEFYVGYEESTAEKRRLLWWKLY   600
IS556_PDR1       EHLLLLLEEQLALDEYYGFEKVLNVAVANAKKMGFHRWEFYVGYEESTAEKRRLLWWKLY   600
                 ************************************************************

CBS138_PDR1      NYEKASTMKKGFFSVIDDATVNCLLPKIFRNFGYLDRVEFLENIQKPMDLSVFSDVPISV   660
IS556_PDR1       NYEKASTMKKGFFSVIDDATVNCLLPKIFRNFGYLDRVEFLENIQKPMDLSVFSDVPISV   660
                 ************************************************************

CBS138_PDR1      LCKYGELALTIVTSEFHEKFLYADRYTSIRNSAKPPTLKNQLIKEIVDGIAYTETSYEAI   720
IS556_PDR1       LCKYGELALTIVTSEFHEKFLYADRYTSIRNSAKPPTLKNQLIKEIVDGIAYTETSYEAI   720
                 ************************************************************

CBS138_PDR1      RKQTAKLWDIALGKVTKDKINKEDTAAASKFTLSYEYHRFRLINMADNLIARLMVKPKSD   780
IS556_PDR1       RKQTAKLWDIALGKVTKDKINKEDTAAASKFTLSYEYHRFRLINMADNLIARLMVKPKSD   780
                 ************************************************************

CBS138_PDR1      WLISVMKGHLNRLYEHWKVMNEIILSMDNDYSIATTFEYYAPSCLCLATQTFLIVRNMEM   840
IS556_PDR1       WLISVMKGHLNRLYEHWKVMNEIILSMDNDYSIATTFEYYAPSCLCLATQTFLIVRNMEM   840
                 ************************************************************

CBS138_PDR1      DDVKMMVAVYKRFLNLGMFLQSAKVCSLADSHTFRDFSRSFSFITIISRLMIIEFMQIKE   900
IS556_PDR1       DDVKMMVAVYKRFLNLGMFLQSAKVCSLADSHTFRDFSRSFSFITIISRLMIIEFMQIKE   900
                 ************************************************************

CBS138_PDR1      LTKVEFIEKFSEVCPDLADLPPMLLDPNSCLYFSLLQQIKKSGFTLSFKKILEDARMMDF   960
IS556_PDR1       LTKVEFIEKFSEVCPDLADLPPMLLDPNSCLYFSLLQQIKKSGFTLSFKKILEDARMMDF   960
                 ************************************************************

CBS138_PDR1      NYDRNLDSEAIKKCNGEFSKSMPSCTNVSDTTTAVSDNSAKKKASMGSARVNSTDTLTAS   1020
IS556_PDR1       NYDRNLDSEAIKKCNGEFSKSMPSCTNVSDTTTAVSDNSAKKKASMGSARVNSTDTLTAS   1020
                 ************************************************************

CBS138_PDR1      PLSGLRNQTQLDSKDSVPSLEAYTPIDSVSDVPTGEINVPFPPVYNQNGLDQQTTYNLGT   1080
IS556_PDR1       PLSGLRNQTQLDSKDSVPSLEAYTPIDSVSDVPTGEINVPFPPVYNQNGLDQQTTYNLGT   1080
                 ************************************************************

CBS138_PDR1      LDEFVNKGDLNELYNSLWGDLFSDVYL    1107
IS556_PDR1       LDEFVNKGDLNELYNSLWGDLFSDVYL    1107
                 ***************************
```

Figure 6.3 - Alignment of the *CgPDR1* sequence obtained from isolate FFUL556 with the sequence of the CBS138 reference strain. The sequencing reaction was performed by STABVIDA as a paid service and Clustal Omega was used for sequence alignment. Amino acid substitutions are represented by a red rectangle.

Annex E

```
CBS138_PDR1      MQTLETTSKSNPGEVKAQKPSTRRTKVGKACDSCRRRKIKCNGLKPCPSCTIYGCECTYT   60
IS607_PDR1       MQTLETTSKSNPGEVKAQKPSTRRTKVGKACDSCRRRKIKCNGLKPCPSCTIYGCECTYT   60
                 ************************************************************

CBS138_PDR1      DAKSTKNLKSNDAGKSKPTGRVSKNKETTHVDKDIRKIEQQYVPINANIHVGPRFPSENI   120
IS607_PDR1       DAKSTKNLKSNDAGKSKPTGRVSKNKETTRIDKDIRKSEQQYVPINANIHVGPRFPSENI   120
                 ******************************:*****.**********************

CBS138_PDR1      LNGYPQCGAPQNNVVGNPLAVNTQCHRGLSETPMSSTFKESNLRDDRLLQSSDTDDMRNG   180
IS607_PDR1       LNGYPQCGAPQNNVVGNPLAVNTQCHRGLSETPMSSTFKESNLRDDRLLQSSDTDDMRNG   180
                 ************************************************************

CBS138_PDR1      DSEERDLKGSDSENVKSKDNKSDPLIIYKDDTHIESTVNKLTQAVNELKSLQNAPSSIKS   240
IS607_PDR1       DSEERDLKGSDSENVKSKDNKSDPLIIYKDDTHIESTVNKLTQAVNELKSLQNAPSSIKS   240
                 ************************************************************

CBS138_PDR1      SIDAIELQLRNILDNWKPEVDFEKAKINESATTKSLETNLLRNKYTNHVHLTRFRIWIDY   300
IS607_PDR1       SINAIELQLRNILDNWKPEVDFEKAKINESATTKSLETNLLRNKYTNHVHLTRFRIWIDY   300
                 **:*********************************************************

CBS138_PDR1      KNANKNNHFMGECGFSLAESFFASNQPLVDELFGLYSQVEAFSLQGLGYCVHLYEPYMKT   360
IS607_PDR1       KNANKNNHFMGECGFSLAESFFASNQPLVDELFGLYSQVEAFSLQGLGYCVHLYEPYMKT   360
                 ************************************************************

CBS138_PDR1      EEAIKLMKETLYIILRFIDICVHHINEESISIANPLETYLRKKHLMPMTPTPRSSYGSPQ   420
IS607_PDR1       EEAIKLMKETLYIILWFIDICVHHINEESISIANPLETYLRKKHLMPMTPTPRSSYGSPQ   420
                 **************.*********************************************

CBS138_PDR1      SASTKSLVSKIIERIPQPFIESVTNVSSLQLLDLRDDESKMFGTLLNMCKSIRRKFDSVM   480
IS607_PDR1       SASTKSLVSKIIERIPQPFIESVTNVSSLQLLDLRDDESKMFGTLLNMCKSIRRKFDSVM   480
                 ************************************************************

CBS138_PDR1      SDYDSIVTEKSEGEQNDGKVTVAEFTSLCEAEEMLLALCYNYYNLTLYSFFEFGTNIEYM   540
IS607_PDR1       SDYDSIVTEKSEGEQNDGKVTVAEFTSLCEAEEMLLALCYNYYNLTLYSFFEFGTNIEYM   540
                 ************************************************************

CBS138_PDR1      EHLLLLLEEQLALDEYYGFEKVLNVAVANAKKMGFHRWEFYVGYEESTAEKRRLLWWKLY   600
IS607_PDR1       EHLLLLLEEQLALDEYYGFEKVLNVAVANAKKMGFHRWEFYVGYEESTAEKRRLLWWKLY   600
                 ************************************************************

CBS138_PDR1      NYEKASTMKKGFFSVIDDATVNCLLPKIFRNFGYLDRVEFLENIQKPMDLSVFSDVPISV   660
IS607_PDR1       NYEKASTMKKGFFSVIDDATVNCLLPKIFRNFGYLDRVEFLENIQKPMDLSVFSDVPISV   660
                 ************************************************************

CBS138_PDR1      LCKYGELALTIVTSEFHEKFLYADRYTSIRNSAKPPTLKNQLIKEIVDGIAYTETSYEAI   720
IS607_PDR1       LCKYGELALTIVTSEFHEKFLYADRYTSIRNSAKPPTLKNQLIKEIVDGIAYTETSYEAI   720
                 ************************************************************

CBS138_PDR1      RKQTAKLWDIALGKVTKDKINKEDTAAASKFTLSYEYHRFRLINMADNLIARLMVKPKSD   780
IS607_PDR1       RKQTAKLWDIALGKVTKDKINKEDTAAASKFTLSYEYHRFRLINMADNLIARLMVKPKSD   780
                 ************************************************************

CBS138_PDR1      WLISVMKGHLNRLYEHWKVMNEIILSMDNDYSIATTFEYYAPSCLCLATQTFLIVRNMEM   840
IS607_PDR1       WLISVMKGHLNRLYEHWKVMNEIILSMDNDYSIATTFEYYAPSCLCLATQTFLIVRNMEM   840
                 ************************************************************

CBS138_PDR1      DDVKMMVAVYKRFLNLGMFLQSAKVCSLADSHTFRDFSRSFSFITIISRLMIIEFMQIKE   900
IS607_PDR1       DDVKMMVAVYKRFLNLGMFLQSAKVCSLADSHTFRDFSRSFSFITIISRLMIIEFMQIKE   900
                 ************************************************************

CBS138_PDR1      LTKVEFIEKFSEVCPDLADLPPMLLDPNSCLYFSLLQQIKKSGFTLSFKKILEDARMMDF   960
IS607_PDR1       LTKVEFIEKFSEVCPDLADLPPMLLDPNSCLYFSLLQQIKKSGFTLSFKKILEDARMMDF   960
                 ************************************************************

CBS138_PDR1      NYDRNLDSEAIKKCNGEFSKSMPSCTNVSDTTTAVSDNSAKKKASMGSARVNSTDTLTAS   1020
IS607_PDR1       NYDRNLDSEAIKKCNGEFSKSMPSCTNVSDTTTAVSDNSAKKKASMGSARVNSTDTLTAS   1020
                 ************************************************************

CBS138_PDR1      PLSGLRNQTQLDSKDSVPSLEAYTPIDSVSDVPTGEINVPFPPVYNQNGLDQQTTYNLGT   1080
IS607_PDR1       PLSGLRNQTQLDSKDSVPSLEAYTPIDSVSDVPTGEINVPFPPVYNQNGLDQQTTYNLGT   1080
                 ************************************************************

CBS138_PDR1      LDEFVNKGDLNELYNSLWGDLFSDVYL    1107
IS607_PDR1       LDEFVNKGDLNELYNSLWGDLFSDVYL    1107
                 ***************************
```

Figure 6.4 - Alignment of the *CgPDR1* sequence obtained from isolate FFUL607 with the sequence of the CBS138 reference strain. The sequencing reaction was performed by STABVIDA as a paid service and Clustal Omega was used for sequence alignment. Amino acid substitutions are represented by a red rectangle.

Annex F

Table 6.2 - List of transformed strains obtained upon insertion of the wild-type or mutated pSP76 vector into *S. cerevisiae* BY4741, *S. cerevisiae* BY4741 Δ*pdr1*, *C. glabrata* Cg66032 or *C. glabrata* SKY107.

Strain transformed	Vector inserted	Resulting transformant
S. cerevisiae BY4741	pSP76	*S. cerevisiae* WT + CgPdr1^{WT}
	pSP76_E5K	*S. cerevisiae* WT + CgPdr1^{E5K}
	pSP76_R35K	*S. cerevisiae* WT + CgPdr1^{R35K}
	pSP76_K274Q	*S. cerevisiae* WT + CgPdr1^{K274Q}
	pSP76_I392M	*S. cerevisiae* WT + CgPdr1^{I392M}
S. cerevisiae BY4741 Δpdr1	pSP76	*S. cerevisiae* Δpdr1 + CgPdr1^{WT}
	pSP76_E5K	*S. cerevisiae* Δpdr1 + CgPdr1^{E5K}
	pSP76_R35K	*S. cerevisiae* Δpdr1 + CgPdr1^{R35K}
	pSP76_K274Q	*S. cerevisiae* Δpdr1 + CgPdr1^{K274Q}
	pSP76_I392M	*S. cerevisiae* Δpdr1 + CgPdr1^{I392M}
C. glabrata Cg66032	pSP76	*C. glabrata* WT + CgPdr1^{WT}
	pSP76_E5K	*C. glabrata* WT + CgPdr1^{E5K}
	pSP76_R35K	*C. glabrata* WT + CgPdr1^{R35K}
	pSP76_K274Q	*C. glabrata* WT + CgPdr1^{K274Q}
	pSP76_I392M	*C. glabrata* WT + CgPdr1^{I392M}
C. glabrata SKY107	pSP76	*C. glabrata* Δpdr1 + CgPdr1^{WT}
	pSP76_E5K	*C. glabrata* Δpdr1 + CgPdr1^{E5K}
	pSP76_R35K	*C. glabrata* Δpdr1 + CgPdr1^{R35K}
	pSP76_K274Q	*C. glabrata* Δpdr1 + CgPdr1^{K274Q}
	pSP76_I392M	*C. glabrata* Δpdr1 + CgPdr1^{I392M}

Annex G

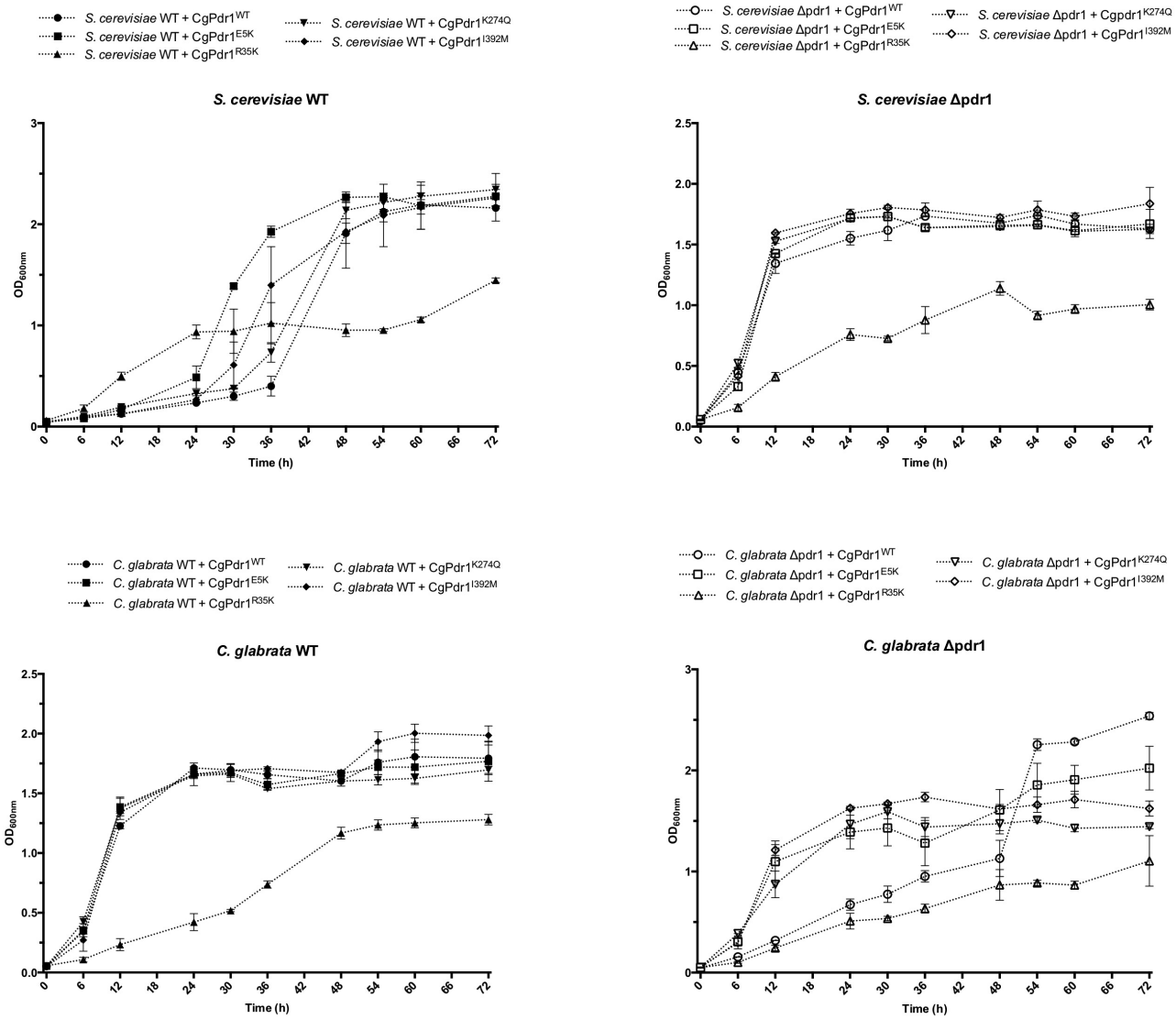

Figure 6.5 - Growth curves of the various *S. cerevisiae* and *C. glabrata* transformants, wild-type and Δ*pdr1* mutant variants, when in the absence of fluconazole.